*Asian European Journal of Probability and Statistics*
Vol. 2, No's. 1-2 (2025), pp. 01-35


# A Parsimonious Transformation within the T–X Family: Applications to Survival, Hydrological, and COVID-19 Data

Sini K P[a], Davis Antony Mundassery[b], and V M Chacko[a]

[a] *Department of Statistics, St. Thomas College (Autonomous), affiliated to the University of Calicut, Thrissur, 680 001, Kerala, India.* [b] *Department of Statistics, Christ College (Autonomous), affiliated to the University of Calicut, Irinjalakkuda, 680 125, Kerala, India.*

**ARTICLE HISTORY**
Compiled December 2, 2025

Received 19 December 2024; Accepted 09 August 2025

**ABSTRACT**
This paper introduces a new parsimonious transformation within the T-X family of distributions that generates flexible models without introducing additional parameters. The proposed generator enhances classical distributions by embedding a structurally adaptive mechanism capable of modeling diverse hazard rate shapes—including increasing, decreasing, and bathtub forms—while maintaining computational simplicity. Analytical properties such as linear representation, moments, order statistics, and information-theoretic measures are systematically derived and examined. Maximum likelihood estimation procedures are developed, and a Monte Carlo simulation study evaluates estimator performance under varying sample sizes and parameter settings through bias, mean squared error, and coverage probability. Two submodels—the New Parsimonious Exponential (NPEx) and New Parsimonious Weibull (NPW) distributions—are explored in detail. Their flexibility is demonstrated through visualization, parameter sensitivity analysis, and empirical validation using three real-world datasets: COVID-19 case counts from Kerala (India), flood peak exceedances from the Wheaton River (Canada), and leukemia patient survival times. Model comparison using goodness-of-fit criteria (AIC, BIC, CAIC, HQIC) and the Nikulin–Rao–Robson statistic confirms that the proposed family achieves superior fit with minimal parameterization, providing a unified and robust framework for lifetime and reliability modeling.

**KEYWORDS**
T–X family of distributions; Parameter-preserving transformation; Survival analysis; Hydrological modeling; Kerala COVID-19 data; N.R.R statistic

## 1. Introduction

In recent years, the development of transformation-based distribution families has provided a unifying framework for constructing flexible probability models across diverse applied domains. Among these, the T–X family of distributions [3] has gained prominence due to its ability to generate new continuous distributions through functional transformations of a baseline cumulative distribution function (*cdf*). These methods allow researchers to tailor models to accommodate skewness, kurtosis, and complex haz-

CONTACT Sini K P & Davis Antony[a]. Email:sinikpstat@gmail.com; dmundassery@christcollegeijk.edu.in

ard structures observed in real-world data. However, many generalizations achieve flexibility by introducing additional shape parameters, which can complicate estimation and interpretation. In contrast, parameter-preserving transformations (PPT), those that retain the parameter dimensionality of the baseline distribution (BD), offer a parsimonious alternative with comparable adaptability. This paper contributes to this stream of research by examining a specific PPT within the T–X framework, defined by $G(x) = F(x)e^{1-F(x)}$, and by demonstrating its analytical properties and practical utility through applications to survival, hydrological, and epidemiological data.

The motivation for this work arises from the practical need for models that balance flexibility and interpretability when describing real-world phenomena such as survival lifetimes, hydrological extremes, and epidemiological growth patterns. Although many transformation-based families offer substantial shape adaptability, this often comes at the cost of additional parameters that complicate inference and limit practical usability in small or moderate samples. The present study focuses on a parsimonious alternative that maintains the parameter dimensionality of the BD while still accommodating diverse data behaviors. Specifically, the transformation $G(x) = F(x)e^{1-F(x)}$ is examined as a parameter-preserving member of the T–X family. The objectives of this paper are threefold: (i) to derive and analyze its key distributional properties, including the probability density, survival, hazard, and quantile functions; (ii) to investigate the behavior of maximum likelihood estimators through simulation under finite samples; and (iii) to demonstrate the transformation's practical utility using empirical applications to survival, hydrological, and COVID-19 datasets.

The proposed transformation builds upon a broad body of research on generator-based families of continuous distributions. Early contributions such as the *Transmuted–G* family [25] and its subsequent extensions [4, 19] introduced functional transformations to enhance baseline models. Parallel developments produced the *Exponentiated–G*, *Beta–G*, and *Kumaraswamy–G* families [11, 13, 8], which achieved additional flexibility through the inclusion of extra shape parameters. The *T–X family* unified many of these generator approaches by expressing new models as monotonic transformations of an existing *cdf*, inspiring further variants such as [5] and [26]. More recently, parsimonious or PPT have been investigated as means to maintain interpretability while preserving the ability to capture diverse data behaviors [10, 16]. Within this context, the transformation $G(x) = F(x)e^{1-F(x)}$ exemplifies a simple parameter-preserving member of the T–X framework, complementing existing methods by providing distributional flexibility through its functional structure rather than by introducing additional parameters.

The remainder of the paper is organized as follows. Section 2 presents the analytical formulation of the proposed transformation within the T–X framework. The key distributional properties, including the probability density, survival, and hazard functions, together with analytical representations for moments and entropy, are discussed in Section 3. Section 4 outlines the maximum likelihood estimation (MLE) procedure. Section 5 examines in detail two submodels based on the exponential and Weibull distributions. Section 6 demonstrates the practical relevance of the proposed transformation through empirical analyses using three real-world datasets from survival, hydrological, and epidemiological contexts. The goodness-of-fit evaluation based on the Nikulin–Rao–Robson (NRR) test statistic is provided in Section 7. Finally, Section 8 summarizes the principal findings, highlights the advantages of parameter-preserving transformations for applied modeling, and suggests directions for future research.

## 2. Methodology

This section presents the analytical formulation of the proposed PPT within the T–X framework. Let $F(y;\boldsymbol{\zeta})$ denote a baseline *cdf* with corresponding probability density function (*pdf*) $f(x;\boldsymbol{\zeta})$, where $\boldsymbol{\zeta}$ is the vector of baseline parameters. The proposed, transformed *cdf* is defined as

$$G(y;\boldsymbol{\zeta}) = F(y;\boldsymbol{\zeta})\, e^{\,1-F(y;\boldsymbol{\zeta})}, \tag{1}$$

which satisfies the regularity conditions $G(-\infty) = 0$, $G(\infty) = 1$, and $G'(y) > 0$ for all $y$. This construction represents a specific functional case of the general T–X transformation

$$G(y) = W(F(y)),$$

with $W(u) = ue^{\,1-u}$, where $W : [0,1] \to [0,1]$ is continuous, increasing, and concave. The concavity of $W(u)$ ensures that the resulting distribution is stochastically smaller than the baseline, effectively reallocating probability mass toward the lower tail.

## 3. Structural Properties

### *3.1. Probability Density and Survival Functions*

Differentiating (1) with respect to $y$ yields the *pdf*

$$g(y;\boldsymbol{\zeta}) \;=\; f(y;\boldsymbol{\zeta})\, T\big(F(y;\boldsymbol{\zeta})\big), \qquad T(u) \;=\; W'(u) \;=\; e^{\,1-u}\,(1-u), \;\; 0<u<1, \tag{2}$$

where $f(y;\boldsymbol{\zeta})$ is the baseline *pdf* and $W(u) = u\, e^{\,1-u}$ is the generating function. For computational convenience, we also write the reweighting in the shorthand form

$$g(y;\boldsymbol{\zeta}) \;=\; f(y;\boldsymbol{\zeta})\, M(y;\boldsymbol{\zeta}), \qquad M(y;\boldsymbol{\zeta}) \;=\; T\big(F(y;\boldsymbol{\zeta})\big) \;=\; e^{\,1-F(y;\boldsymbol{\zeta})}\,\{1-F(y;\boldsymbol{\zeta})\}. \tag{3}$$

Since $T(u) > 0$ for $0 < u < 1$ and

$$\int_0^1 T(u)\, du \;=\; \int_0^1 e^{\,1-u}\,(1-u)\, du \;=\; 1, \tag{4}$$

$g(y;\boldsymbol{\zeta})$ is nonnegative and integrates to unity, so $G(y;\boldsymbol{\zeta})$ defines a valid *cdf* for any continuous baseline $F(y;\boldsymbol{\zeta})$.

The survival function and hazard rate of the transformed model are

$$\bar{G}(y;\boldsymbol{\zeta}) \;=\; 1 - F(y;\boldsymbol{\zeta})\, e^{\,1-F(y;\boldsymbol{\zeta})}, \tag{5}$$

$$h_G(y;\boldsymbol{\zeta}) \;=\; \frac{g(y;\boldsymbol{\zeta})}{\bar{G}(y;\boldsymbol{\zeta})} \;=\; \frac{e^{\,1-F(y;\boldsymbol{\zeta})}\,\{1-F(y;\boldsymbol{\zeta})\}\, f(y;\boldsymbol{\zeta})}{1-F(y;\boldsymbol{\zeta})\, e^{\,1-F(y;\boldsymbol{\zeta})}}. \tag{6}$$

Let $S(y;\boldsymbol{\zeta}) = 1-F(y;\boldsymbol{\zeta})$ denote the baseline survival and $h_F(y;\boldsymbol{\zeta}) = f(y;\boldsymbol{\zeta})/S(y;\boldsymbol{\zeta})$

the baseline hazard. Then the transformed hazard admits the product form

$$h_G(y;\boldsymbol{\zeta}) \;=\; h_F(y;\boldsymbol{\zeta})\,\Phi\big(F(y;\boldsymbol{\zeta})\big), \qquad \Phi(F) \;=\; \frac{e^{\,1-F}\,(1-F)^2}{1-F\,e^{\,1-F}}\,, \tag{7}$$

or, equivalently, in terms of $S$,

$$h_G(y;\boldsymbol{\zeta}) \;=\; h_F(y;\boldsymbol{\zeta})\,\Psi\big(S(y;\boldsymbol{\zeta})\big), \qquad \Psi(S) \;=\; \frac{e^{\,S}\,S^2}{1-(1-S)\,e^{\,S}}\,. \tag{8}$$

This factorization shows that the proposed hazard equals the baseline hazard multiplied by a smooth, parameter-free adjustment depending only on the baseline cumulative (or survival) probability. Because $\Phi(F) > 1$ for small $F$ and $\Phi(F) < 1$ for large $F$, the transformation typically amplifies early hazards while attenuating tail hazards, enabling monotonic and non-monotonic shapes (including bathtub and unimodal patterns) without introducing additional parameters.

### *3.2. Quantile Function and Random Variate Generation*

The quantile function (qf) provides a convenient analytic tool for both theoretical characterization and random variate generation. Let $u = F(y;\boldsymbol{\zeta})$ and $p = G(y;\boldsymbol{\zeta})$. From (1), we obtain

$$p = u\,e^{\,1-u} \quad\Longleftrightarrow\quad u\,e^{-u} = \frac{p}{e}. \tag{9}$$

Multiplying both sides by $-1$ and applying the Lambert $W$ function, defined implicitly by $W(z)e^{W(z)} = z$, yields

$$u = -\,W_0\Big(-\frac{p}{e}\Big)\,, \tag{10}$$

where $W_0(\cdot)$ denotes the principal branch of the Lambert $W$ function. Substituting this expression into the baseline qf $F^{-1}(\cdot)$ gives

$$Q_G(p;\boldsymbol{\zeta}) = F^{-1}\Big[-\,W_0\Big(-\frac{p}{e}\Big)\,;\,\boldsymbol{\zeta}\Big]\,, \qquad 0 < p < 1. \tag{11}$$

Equation (11) shows that the quantile of the transformed model is obtained by evaluating the baseline quantile at a rescaled cumulative probability, where the rescaling is governed by the Lambert $W$ function. This relationship also permits random variate generation as follows:

(1) Generate $U \sim \text{Uniform}(0,1)$;
(2) Compute $u^* = -W_0(-U/e)$;
(3) Obtain $Y = F^{-1}(u^*;\boldsymbol{\zeta})$.

The boundary conditions are consistent with a valid *cdf*: as $p \to 0$, $u \to 0$ and $Q_G(p) \to -\infty$; as $p \to 1$, $u \to 1$ and $Q_G(p) \to \infty$, so the transformation preserves the support of the BD.

Because the Lambert $W$ function is implemented in standard scientific software (`lambertW` in `R`, `scipy.special.lambertw` in Python, `LambertW` in `Mathematica`),

the above procedure enables efficient simulation from the proposed transformation. Moreover, the analytic form of $Q_G(p;\boldsymbol{\zeta})$ facilitates the derivation of L-moments and quantile-based measures of skewness and kurtosis, offering additional avenues for characterizing distributional shape and variability.

### *3.3. Linear Representation*

To facilitate subsequent derivations, we express the proposed density as an infinite linear mixture of exponentiated–$G$ (Ex-G) components. Recall that

$$g(y;\boldsymbol{\zeta}) = f(y;\boldsymbol{\zeta})\, e^{\,1-F(y;\boldsymbol{\zeta})}\,\{1-F(y;\boldsymbol{\zeta})\}, \qquad F \equiv F(y;\boldsymbol{\zeta}),\ f \equiv f(y;\boldsymbol{\zeta}).$$

Using the expansions $e^{-F} = \sum_{m=0}^{\infty} \frac{(-F)^m}{m!}$ and $(1-F) = 1-F$, we obtain

$$e^{\,1-F}(1-F) = e\left[1+\sum_{j=1}^{\infty} b_j\, F^j\right], \qquad b_j = (-1)^j\left(\frac{1}{j!}+\frac{1}{(j-1)!}\right),\ j \geq 1,$$

(with $b_0 = 1$). Therefore,

$$g(y;\boldsymbol{\zeta}) = f\, e\left[1+\sum_{j=1}^{\infty} b_j\, F^j\right] = \sum_{j=0}^{\infty} a_j\, q_{j+1}(y;\boldsymbol{\zeta}), \tag{12}$$

where

$$q_{j+1}(y;\boldsymbol{\zeta}) = (j+1)\, F(y;\boldsymbol{\zeta})^j\, f(y;\boldsymbol{\zeta})$$

is the Ex–$G$ density with power parameter $(j+1) > 0$, and the mixture weights are

$$a_0 = \frac{e}{1}, \qquad a_j = \frac{e\, b_j}{j+1} = \frac{e\,(-1)^j}{j+1}\left(\frac{1}{j!}+\frac{1}{(j-1)!}\right), \quad j \geq 1.$$

Integrating (12) gives the corresponding representation for the *cdf* as

$$G(y;\boldsymbol{\zeta}) = \sum_{j=0}^{\infty} a_j\, Q_{j+1}(y;\boldsymbol{\zeta}),$$

where $Q_{j+1}(\cdot;\boldsymbol{\zeta})$ is the *cdf* of the Ex–$G$ family with power $(j+1)$.

#### *3.3.1. Remarks*

(i) The factorial terms in $a_j$ guarantee absolute convergence of the series for all $y$ (uniform on compact sets in $F$), making the linear representation (LR) numerically stable for truncation.
(ii) The LR shows that many analytical functionals of the proposed model can be obtained by reusing known formulas for the Ex–$G$ class (e.g., moment integrals reduce to weighted sums of Ex–$G$ moments).

### *3.4. Moments, Generating Functions, and Entropy*

Analytical characterisation of the proposed model can be advanced through its moment and information–theoretic properties. Let $Y$ denote a random variable (RV) following (1) with BD $F(y;\boldsymbol{\zeta})$ and corresponding density $f(y;\boldsymbol{\zeta})$. Using the representation in (3), the $r^{th}$ raw moment is

$$\mu'_r = \mathrm{E}[Y^r] = \int_{-\infty}^{\infty} y^r \, f(y;\boldsymbol{\zeta}) \, M(y;\boldsymbol{\zeta}) \, dy. \tag{13}$$

By the change of variable $u = F(y;\boldsymbol{\zeta})$, $du = f(y;\boldsymbol{\zeta})\, dy$, we obtain the compact form

$$\mu'_r = \int_0^1 Q_F(u;\boldsymbol{\zeta})^r \, e^{\,1-u}(1-u) \, du, \tag{14}$$

where $Q_F(\cdot)$ is the baseline qf. Equation (14) shows that the transformation preserves the support of the baseline model while weighting the qf by $e^{\,1-u}(1-u)$. When $Q_F(u)$ is available in closed form (e.g. exponential or Weibull baselines), the integral can be expressed analytically; otherwise, numerical quadrature provides accurate estimates.

#### *3.4.1. Moment and Cumulant Generating Functions*

Using the LR in Section 3.3, the moment generating function (MGF) can be written as a weighted sum of MGFs of Ex-$G$ densities.

$$M_Y(t) = \sum_{j=0}^{\infty} a_j \, M_{j+1}(t), \qquad M_{j+1}(t) = \int_{-\infty}^{\infty} e^{ty} \, q_{j+1}(y;\boldsymbol{\zeta}) \, dy, \tag{15}$$

where $a_j$ and $q_{j+1}(\cdot)$ are defined in (12). The cumulant generating function (CGF) is $K_Y(t) = \ln M_Y(t)$, and the $r^{th}$ cumulant $\kappa_r$ follows by differentiation at $t = 0$.

#### *3.4.2. Central Moments and Shape Measures*

Central moments follow in the usual way, $\mu_r = \mathrm{E}[(Y - \mu'_1)^r]$, with variance $\sigma^2 = \mu_2$ and coefficient of skewness $\gamma_1 = \mu_3/\sigma^3$. Because the weighting function $e^{\,1-u}(1-u)$ shifts probability mass toward smaller $u$, the transformation typically increases right skewness and can slightly reduce variance relative to the baseline, depending on the tail behaviour of $F$.

#### *3.4.3. Entropy*

The Shannon entropy of the transformed model is

$$\begin{aligned} H_G &= -\int_{-\infty}^{\infty} g(y;\boldsymbol{\zeta}) \, \ln g(y;\boldsymbol{\zeta}) \, dy \\ &= -\int_0^1 e^{\,1-u}(1-u) \ln\Big[e^{\,1-u}(1-u) \, f(Q_F(u;\boldsymbol{\zeta});\boldsymbol{\zeta})\Big] du. \end{aligned} \tag{16}$$

The second expression separates the baseline contribution from that of the transformation. Because $e^{\,1-u}(1-u) < 1$ for $u > 0$, the entropy of the new distribution is

generally smaller than that of the baseline, reflecting the reduction in uncertainty associated with its left-shifted mass.

### *3.5. Shape Properties of the PDF and Hazard Function*

An essential aspect of any generated family is its ability to capture a wide range of shapes for the density and hazard functions. The proposed transformation, being parameter–preserving, modifies the baseline shape exclusively through the functional factor $M(y;\boldsymbol{\zeta})$, without altering the parameter space. This section examines the analytical conditions under which the transformed model produces monotonic, unimodal, or non–monotonic forms.

#### *3.5.1. Critical points of the density*

Differentiating (3) yields

$$g'(y;\boldsymbol{\zeta}) = e^{\,1-F(y;\boldsymbol{\zeta})}\Big[-f(y;\boldsymbol{\zeta})^2\{1-F(y;\boldsymbol{\zeta})\} + \{1-2F(y;\boldsymbol{\zeta})\}f'(y;\boldsymbol{\zeta})\Big]. \tag{17}$$

Setting $g'(y;\boldsymbol{\zeta}) = 0$ gives the stationary points satisfying

$$\frac{f'(y;\boldsymbol{\zeta})}{f(y;\boldsymbol{\zeta})} = \frac{f(y;\boldsymbol{\zeta})\{1-F(y;\boldsymbol{\zeta})\}}{1-2F(y;\boldsymbol{\zeta})}. \tag{18}$$

Equation (18) links the slope of the baseline log–density to its cumulative function and reveals how the transformation shifts the location of the mode. For $F(y) < \frac{1}{2}$, the right–hand side is positive, suggesting that the peak of $g(y)$ occurs at smaller values of $y$ relative to the baseline, confirming a leftward shift of the mass.

#### *3.5.2. Shape of the hazard function*

From (7), the derivative of the hazard is

$$\frac{dh_G(y;\boldsymbol{\zeta})}{dy} = h'_F(y;\boldsymbol{\zeta})\,\Phi(F) + h_F(y;\boldsymbol{\zeta})\,f(y;\boldsymbol{\zeta})\,\Phi'(F), \tag{19}$$

where

$$\Phi'(F) = e^{\,1-F}\left[\frac{-F(1-F)^2 + 2(1-F)(1-Fe^{\,1-F})}{(1-Fe^{\,1-F})^2}\right].$$

Since $\Phi'(F)$ changes sign as $F$ increases, the proposed model can produce both increasing and decreasing segments in $h_G(y)$, leading to non–monotonic hazard shapes such as bathtub or inverse–bathtub forms. The inflection points occur where $\Phi'(F) = 0$, approximately around $F \approx 0.3$ and $F \approx 0.8$, depending on the baseline form.

### *3.6. Stochastic Ordering*

The concavity of the generating function $W(u) = ue^{1-u}$ implies that $W(u) < u$ for all $u \in (0, 1)$. Consequently,

$$G(y; \boldsymbol{\zeta}) = W(F(y; \boldsymbol{\zeta})) < F(y; \boldsymbol{\zeta}), \qquad \forall\, y.$$

Hence, the transformed variable $Y_G$ is stochastically smaller than the baseline variable $Y_F$, written as $Y_G \leq_{\text{st}} Y_F$. Moreover, since $W'(u) = e^{1-u}(1-u)$ is decreasing in $u$, the model also satisfies $Y_G \leq_{\text{hr}} Y_F$ and $Y_G \leq_{\text{lr}} Y_F$ in the hazard–rate and likelihood–ratio orderings, respectively. These results confirm analytically that the proposed transformation shifts probability mass toward lower values and produces lighter right tails than the BD.

## 4. Parameter Estimation via Maximum Likelihood

The unknown parameters of the proposed model can be estimated by the method of maximum likelihood, which provides efficient and asymptotically normal estimators under standard regularity conditions. Let $y_1, y_2, \ldots, y_n$ denote a random sample of size $n$ from (1) with *pdf* in (2). The log-likelihood function is then

$$\begin{aligned} \ell(\boldsymbol{\zeta}) &= \sum_{i=1}^{n} \ln g(y_i; \boldsymbol{\zeta}) \\ &= \sum_{i=1}^{n} \Big[ \ln f(y_i; \boldsymbol{\zeta}) + 1 - F(y_i; \boldsymbol{\zeta}) + \ln\{1 - F(y_i; \boldsymbol{\zeta})\} \Big]. \end{aligned} \tag{20}$$

The score vector, obtained by differentiating $\ell(\boldsymbol{\zeta})$ with respect to $\boldsymbol{\zeta}$, is

$$\begin{aligned} U(\boldsymbol{\zeta}) &= \frac{\partial \ell(\boldsymbol{\zeta})}{\partial \boldsymbol{\zeta}} \\ &= \sum_{i=1}^{n} \left[ \frac{1}{f(y_i; \boldsymbol{\zeta})} \frac{\partial f(y_i; \boldsymbol{\zeta})}{\partial \boldsymbol{\zeta}} - \frac{\partial F(y_i; \boldsymbol{\zeta})}{\partial \boldsymbol{\zeta}} - \frac{1}{1 - F(y_i; \boldsymbol{\zeta})} \frac{\partial F(y_i; \boldsymbol{\zeta})}{\partial \boldsymbol{\zeta}} \right]. \end{aligned} \tag{21}$$

The maximum likelihood estimates (MLEs), $\hat{\boldsymbol{\zeta}}$, are obtained by solving $U(\boldsymbol{\zeta}) = \mathbf{0}$ numerically. Because the equations generally have no closed–form solution, iterative optimization algorithms such as the Newton–Raphson, Broyden–Fletcher–Goldfarb–Shanno (BFGS), or other quasi–Newton methods are recommended. These routines are readily available in statistical software, including `optim` in `R`, `PROC NLMIXED` in `SAS`, and `scipy.optimize` in `Python`. Convergence can be monitored using the gradient norm or relative change in the log–likelihood between successive iterations.

Once the MLEs are obtained, approximate standard errors follow from the inverse of the observed Fisher information matrix

$$\mathcal{I}(\hat{\boldsymbol{\zeta}}) = -\frac{\partial^2 \ell(\boldsymbol{\zeta})}{\partial \boldsymbol{\zeta}\, \partial \boldsymbol{\zeta}^{\top}}\bigg|_{\boldsymbol{\zeta}=\hat{\boldsymbol{\zeta}}},$$

and asymptotic confidence intervals for each parameter $\zeta_j$ can be constructed as $\hat{\zeta}_j \pm z_{\alpha/2}\,\mathrm{SE}(\hat{\zeta}_j)$, where $\mathrm{SE}(\hat{\zeta}_j) = \sqrt{[\mathcal{I}^{-1}(\hat{\boldsymbol{\zeta}})]_{jj}}$.

To examine the finite-sample performance of the MLEs, a set of Monte Carlo experiments was conducted under the exponential (Ex) and Weibull (W) submodels of the proposed family. For each case, random samples were generated via the quantile function, and the resulting estimates were evaluated in terms of bias, mean–squared error (MSE), and confidence-interval coverage. The detailed design and outcomes of these simulations are presented within the respective submodel sections, where they provide further support for the robustness and numerical stability of the estimation procedure.

## 5. Illustration with Examples

In this section, we explore specific distributions across different supports of RV, including $(0,1), (0,\theta), (0,\infty), (\mu,0)$, and $(-\infty,\infty)$. We consider the Ex, W, Kumaraswamy (Kw), beta, Burr XII (BXII), Gumbel (Gu), logistic (Lo), power function (PF) or generalized uniform, and Pareto (Pa) models as examples. A detailed study of submodels with Ex and W distributions as baseline are respectively in section 5.1 and section 5.2. Other submodels are provided in Table A1.

### *5.1. Exponential Submodel*

We begin by applying the Ex distribution as the baseline distribution, characterized by its *cdf* $F(t;\lambda) = 1 - e^{-\lambda t}; \quad t > 0, \lambda > 0$. For this new parsimonious exponential (NPEx) distribution, the *cdf*, *pdf*, and *hf* are respectively given by

$$G(y;\lambda) = (1 - e^{-\lambda y})e^{e^{-\lambda y}}; \quad y > 0, \quad \lambda > 0, \tag{22}$$

$$g(y;\lambda) = \lambda e^{-2\lambda y} e^{e^{-\lambda y}}; \quad y > 0, \quad \lambda > 0, \tag{23}$$

$$h(y;\lambda) = \frac{\lambda e^{-2\lambda y} e^{e^{-\lambda y}}}{1 - (1 - e^{-\lambda y})e^{e^{-\lambda y}}}; \quad y > 0, \quad \lambda > 0. \tag{24}$$

Figures 1 and 2 present the cumulative, density, and hazard functions of the Ex and NPEx models for selected values of $\lambda$. The NPEx model shows higher early concentration and lighter tails, indicating right-skewed behavior relative to the baseline exponential. The Ex model exhibits constant hazard, whereas the NPEx model allows decreasing and bathtub-shaped hazard structures, demonstrating enhanced flexibility. Figure 3 further presents the parameter sensitivity analysis: panel (a) shows how changes in $\lambda$ affect the shape and tail behavior of the density, while panel (b) illustrates the corresponding variations in the hazard function.

#### *5.1.1. Quantile Function*

The qf of the NPEx model follows directly from the general formulation discussed in Section 3.2. Since the baseline exponential quantile is $Q_F(p;\lambda) = -\frac{1}{\lambda}\ln(1-p)$, the

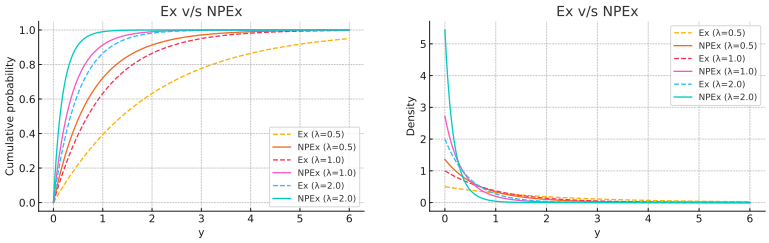


(a) Cumulative distribution functions for Ex and NPEx models at selected values of $\lambda$.

(b) Density functions for Ex and NPEx models at selected values of $\lambda$.

**Figure 1.** Comparison between the Ex and NPEx models for different $\lambda$.

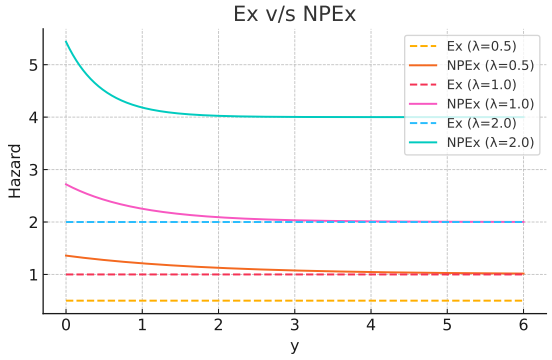


**Figure 2.** Hazard function comparison between the Ex and the NPEx models for different $\lambda$.

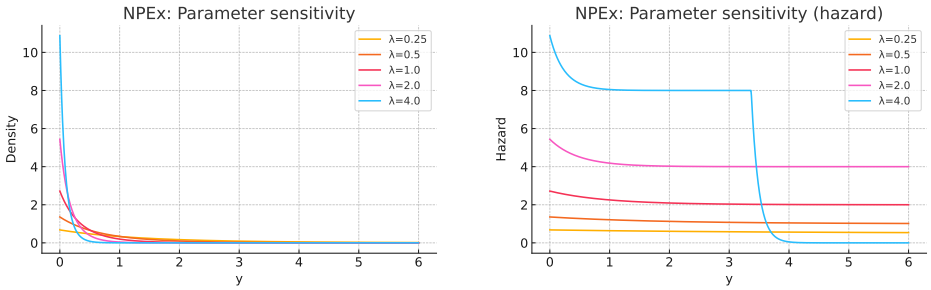


(a) NPEx: Parameter sensitivity (density).

(b) NPEx: Parameter sensitivity (hazard).

**Figure 3.** Parameter sensitivity analysis of the NPEx model for different values of $\lambda$.

inverse relationship yields

$$Q_G(p;\lambda) = F^{-1}\big(-W_0\big(-\tfrac{p}{e}\big)\big) = -\frac{1}{\lambda}\ln\Big(1 + W_0\big(-\tfrac{p}{e}\big)\Big), \qquad 0 < p < 1,$$

where $W_0(\cdot)$ denotes the principal branch of the Lambert $W$ function. This closed-form quantile facilitates random variate generation via the inverse-transform method. When a direct computation of $W_0$ is unavailable, Newton–Raphson iteration can be employed to solve the equation $(1 - e^{-\lambda x})e^{e^{-\lambda x}} - p = 0$ for $x$.

**Algorithm 1** Generation of NPEx Random Variates via Newton–Raphson Inversion

**Require:** Number of variates $n$, parameter $\lambda$
**Ensure:** Array of NPEx random variates $X$

```
for i = 1 to n do
    Generate p_i ~ U(0, 1)
    Choose an initial guess x_0 and tolerance ε
    repeat
        y ← e^{−λx}
        R ← (1 − y)e^y − p_i
        R′ ← λye^y(y − 2)
        x_new ← x − R/R′
        x ← x_new
    until |R| < ε
    X[i] ← x
end for
return X
```

### *5.1.2. Analytical Properties*

Analytical characteristics of the NPEx model can be expressed through its moments and generating functions. Let $Y$ be a RV following the NPEx distribution with parameter $\lambda > 0$ and *pdf* $g(y;\lambda) = \lambda e^{-2\lambda y} e^{e^{-\lambda y}}$.

### *5.1.3. Raw Moments*

The $n^{\text{th}}$ raw moment is defined as

$$\begin{aligned}\mu'_n = \mathrm{E}[Y^n] &= \int_0^\infty x^n g(y;\lambda)\, dy \\ &= \int_0^\infty y^n \lambda e^{-2\lambda y} e^{e^{-\lambda y}}\, dy. \end{aligned} \tag{25}$$

Using the exponential series expansion $e^z = \sum_{m=0}^{\infty} z^m/m!$, we obtain

$$\mu'_n = \sum_{m=0}^{\infty} \frac{\lambda}{m!} \int_0^\infty y^n e^{-\lambda y(m+2)} dy.$$

Recognizing the integral as the Gamma function $\Gamma(n+1)$, we have

$$\mu'_n = \sum_{m=0}^{\infty} \frac{1}{m!} \frac{\Gamma(n+1)}{\lambda^n (m+2)^{n+1}}. \tag{26}$$

Equation (26) provides a convergent series expression that can be truncated for numerical evaluation of the mean, variance, and higher moments.

*5.1.4. MGF*

The MGF $M_Y(t) = \mathrm{E}[e^{tY}]$ is given by

$$\begin{aligned} M_Y(t) &= \int_0^\infty e^{ty} g(y;\lambda)\, dy \\ &= \sum_{m=0}^{\infty} \frac{\lambda}{m!} \int_0^\infty e^{y[t-\lambda(m+2)]} dy, \end{aligned} \tag{27}$$

which converges for $t < \lambda(m+2)$ and simplifies to

$$M_Y(t) = \sum_{m=0}^{\infty} \frac{\lambda}{m![\lambda(m+2) - t]}, \qquad t < 2\lambda. \tag{28}$$

Differentiating $M_Y(t)$ $n$ times and evaluating at $t = 0$ yields the $n^{\text{th}}$ raw moment $\mu'_n = \frac{d^n M_Y(t)}{dt^n}\big|_{t=0}$.

*5.1.5. CF*

The CF $\Phi_Y(t) = \mathrm{E}[e^{itY}]$ has an analogous series form

$$\Phi_Y(t) = \sum_{m=0}^{\infty} \frac{\lambda}{m![\lambda(m+2) - it]}, \qquad t \in \mathbb{R}. \tag{29}$$

Equations (28) and (29) offer compact analytic representations for studying the distribution's moment structure, skewness, and kurtosis. The rapid convergence of the factorial series ensures stable numerical computation even for moderate truncation levels.

*5.1.6. Mean deviation*

The mean absolute deviation about the mean $\mu = \mathbb{E}[X]$ is

$$\begin{aligned} \mathbb{E}[|Y - \mu|] &= \int_0^\infty |y - \mu|\, g(y;\lambda)\, dy \\ &= 2\int_\mu^\infty (y - \mu)\, g(y;\lambda)\, dy \\ &= 2\mu\, G(\mu;\lambda) - 2\mu + 2\int_\mu^\infty x\, g(y;\lambda)\, dy, \end{aligned} \tag{30}$$

where $G(\cdot;\lambda)$ is the NPEx *cdf* and $g(\cdot;\lambda)$ is the NPEx *pdf*. Hence,

$$\mathbb{E}[|Y - \mu|] = 2\mu\big(1 - e^{-\lambda\mu}\big) e^{\,e^{-\lambda\mu}} - 2\mu + 2\int_\mu^\infty y\, \lambda e^{-2\lambda y}\, e^{\,e^{-\lambda y}}\, dy. \tag{31}$$

To evaluate the tail integral, expand $e^{\,e^{-\lambda y}} = \sum_{m=0}^{\infty} \frac{e^{-m\lambda y}}{m!}$ and integrate termwise

$$\begin{aligned}\int_{\mu}^{\infty} y\,\lambda e^{-2\lambda y}\, e^{\,e^{-\lambda y}}\, dy &= \sum_{m=0}^{\infty} \frac{1}{m!} \int_{\mu}^{\infty} \lambda y\, e^{-(m+2)\lambda y}\, dy \\ &= \sum_{m=0}^{\infty} \frac{1}{m!}\, e^{-(m+2)\lambda \mu} \left( \frac{\mu}{m+2} + \frac{1}{(m+2)^2\,\lambda} \right). \end{aligned} \tag{32}$$

Substituting into (31) yields a rapidly convergent series for $\mathbb{E}[|Y-\mu|]$.

*5.1.7. Mean deviation about the median*

Let $M$ be the (unique) median, i.e., $G(M;\lambda) = 1/2$. By the same decomposition,

$$\begin{aligned}\mathbb{E}[|Y-M|] &= 2M\,G(M;\lambda) - 2M + 2\int_{M}^{\infty} y\, g(y;\lambda)\, dy \\ &= -M + 2\int_{M}^{\infty} y\, g(y;\lambda)\, dy, \end{aligned} \tag{33}$$

and the tail integral admits the analogous series

$$\int_{M}^{\infty} y\,\lambda e^{-2\lambda y}\, e^{\,e^{-\lambda y}}\, dy = \sum_{m=0}^{\infty} \frac{1}{m!}\, e^{-(m+2)\lambda M} \left( \frac{M}{m+2} + \frac{1}{(m+2)^2\,\lambda} \right).$$

*5.1.8. Remarks*

(i) The $1/m!$ factors ensure fast numerical convergence; truncation at $m \le 10$–$15$ is typically sufficient.
(ii) The same approach yields mean deviations about any threshold $c > 0$ by replacing $\mu$ (or $M$) with $c$.

*5.1.9. Order statistics*

Let $Y_1, \ldots, Y_n$ be i.i.d. with continuous *cdf* $G(y)$ and *pdf* $g(y)$, and let $Y_{k:n}$ denote the $k^{th}$ order statistic. The distribution functions of $Y_{k:n}$ are

$$G_{k:n}(y) = \Pr(Y_{k:n} \le y) = \sum_{j=k}^{n} \binom{n}{j} \big[G(y)\big]^{j} \big[1-G(y)\big]^{\,n-j}, \tag{34}$$

$$g_{k:n}(y) = \frac{n!}{(k-1)!(n-k)!} \big[G(y)\big]^{k-1} \big[1-G(y)\big]^{\,n-k} g(y). \tag{35}$$

For the NPEx model,

$$G(y;\lambda) = \left(1 - e^{-\lambda y}\right) e^{\,e^{-\lambda y}}, \qquad g(y;\lambda) = \lambda\, e^{-2\lambda y}\, e^{\,e^{-\lambda y}}, \qquad y > 0,\ \lambda > 0.$$

Substituting into (34)–(35) yields

$$G_{k:n}(y;\lambda) = \sum_{j=k}^{n} \binom{n}{j} \Big[\big(1-e^{-\lambda y}\big)\, e^{\,e^{-\lambda y}}\Big]^{j} \Big[1-\big(1-e^{-\lambda y}\big)\, e^{\,e^{-\lambda y}}\Big]^{\,n-j}, \tag{36}$$

$$g_{k:n}(y;\lambda) = \frac{n!}{(k-1)!(n-k)!} \Big[\big(1-e^{-\lambda y}\big)\, e^{\,e^{-\lambda y}}\Big]^{k-1} \Big[1-\big(1-e^{-\lambda y}\big)\, e^{\,e^{-\lambda y}}\Big]^{\,n-k} \lambda\, e^{-2\lambda y}\, e^{\,e^{-\lambda y}}. \tag{37}$$

In particular, the extremes are

$$G_{1:n}(y;\lambda) = 1-\Big[1-G(y;\lambda)\Big]^{n}, \qquad G_{n:n}(y;\lambda) = \big[G(y;\lambda)\big]^{n},$$

with densities obtained from (37) by setting $k=1$ or $k=n$.

*5.1.10. Quantile representation*

Let $Q_G(\cdot;\lambda)$ be the NPEx quantile (Section 5.1.1). For $k=1,\ldots,n$,

$$\mathbb{E}\big[Y_{k:n}\big] = \int_0^1 Q_G(u;\lambda)\, \mathrm{Beta}\big(u;\, k,\, n-k+1\big)\, du,$$

and higher moments follow analogously. This representation is convenient for accurate numerical evaluation because $Q_G$ is available in closed form via the Lambert $W$ function.

*5.1.11. Entropy and information measures*

Entropy quantifies the uncertainty or information content associated with a probability distribution. For a continuous RV $Y$ with *pdf* $g(y)$, the Rényi entropy of order $\delta > 0$ ($\delta \neq 1$) is defined as

$$H_\delta(Y) = \frac{1}{1-\delta} \log\left[\int_0^\infty \big\{g(y;\lambda)\big\}^{\delta}\, dy\right]. \tag{38}$$

For the NPEx distribution, substituting $g(y;\lambda) = \lambda e^{-2\lambda y} e^{\,e^{-\lambda y}}$ gives

$$\begin{aligned}\int_0^\infty \{g(y;\lambda)\}^{\delta}\, dy &= \lambda^{\delta} \int_0^\infty e^{-2\delta\lambda y}\, e^{\delta e^{-\lambda y}}\, dy \\ &= \frac{\lambda^{\delta-1}}{2\delta} \sum_{m=0}^{\infty} \frac{(2\delta)^m}{m!(m+2\delta)},\end{aligned} \tag{39}$$

where the exponential term has been expanded using $e^{\delta e^{-\lambda y}} = \sum_{m=0}^{\infty} \frac{(\delta e^{-\lambda y})^m}{m!}$. Hence the Rényi entropy of the NPEx model can be expressed as

$$H_\delta(Y) = \frac{1}{1-\delta}\left[\log\left(\frac{\lambda^{\delta-1}}{2\delta}\right) + \log\left(\sum_{m=0}^{\infty} \frac{(2\delta)^m}{m!(m+2\delta)}\right)\right]. \tag{40}$$

Equation (40) provides a rapidly convergent series representation that can be truncated for numerical evaluation. The Shannon entropy is obtained in the limit $\delta \to 1$. Figure 4 illustrates the variation of the Rényi entropy with respect to $\delta$ for selected values of $\lambda$.

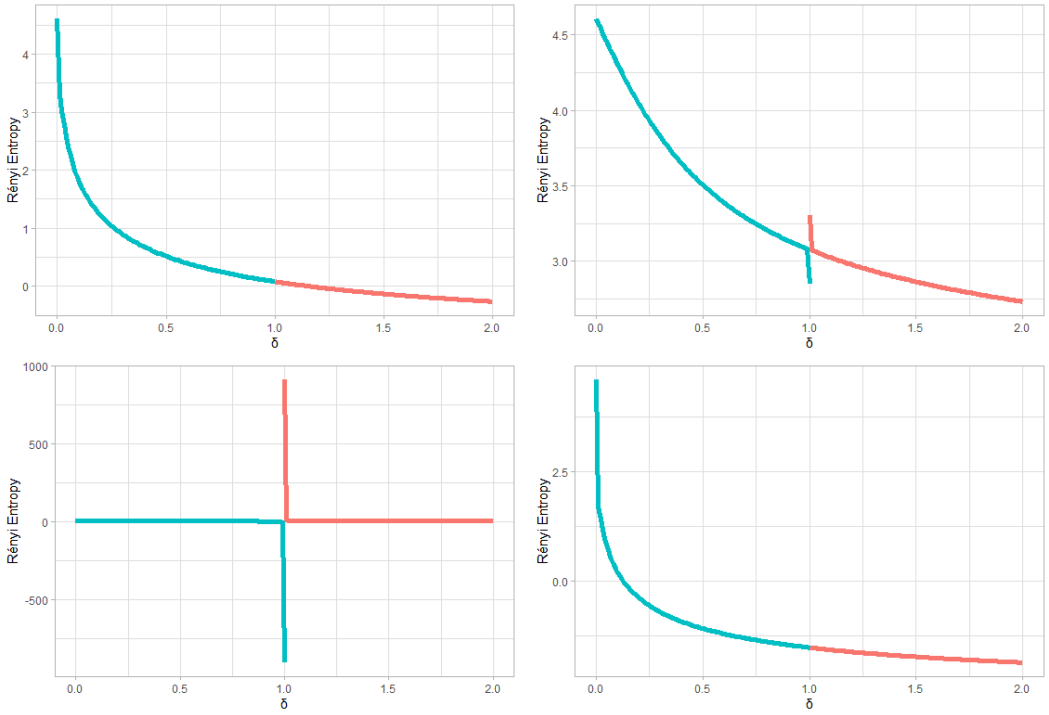


**Figure 4.** NPEx distribution: Rényi entropy for $\lambda = 1$, 0.05, 0.01, and 5. Higher $\lambda$ values lead to lower entropy, reflecting increased concentration of probability near the origin.

### *5.1.12. Estimation*

Let $\{y_1, y_2, \ldots, y_n\}$ be a random sample of size $n$ drawn from the NPEx distribution with parameter $\lambda$. The likelihood function is given by

$$L(\lambda; y_1, y_2, \ldots, y_n) = \prod_{i=1}^{n} g(y_i; \lambda), \qquad g(y; \lambda) = \lambda e^{-2\lambda y} e^{\,e^{-\lambda y}}.$$

Taking logarithms, the log-likelihood function becomes

$$\ell(\lambda) = n \log \lambda - 2\lambda \sum_{i=1}^{n} y_i + \sum_{i=1}^{n} e^{-\lambda y_i}. \tag{41}$$

The score function, obtained by differentiating (41) with respect to $\lambda$, is

$$U(\lambda) = \frac{\partial \ell}{\partial \lambda} = \frac{n}{\lambda} - 2\sum_{i=1}^{n} y_i - \sum_{i=1}^{n} y_i e^{-\lambda y_i}. \tag{42}$$

Setting $U(\lambda) = 0$ gives the MLE $\hat{\lambda}$, which must be found numerically. The observed

Fisher information is obtained from the negative of the second derivative:

$$I(\lambda) = -\frac{\partial^2 \ell}{\partial \lambda^2} = \frac{n}{\lambda^2} - \sum_{i=1}^{n} y_i^2 e^{-\lambda y_i}. \tag{43}$$

The asymptotic variance of $\hat{\lambda}$ is given by $\mathrm{Var}(\hat{\lambda}) \approx I^{-1}(\hat{\lambda})$, and confidence intervals can be constructed using the Wald approach:

$$\hat{\lambda} \pm z_{\alpha/2} \sqrt{\mathrm{Var}(\hat{\lambda})}.$$

The nonlinear score in (42) is solved iteratively using standard numerical routines such as the Newton–Raphson or BFGS algorithms. In this study, all numerical optimizations were implemented in R [22] using the `optim` function.

### *5.1.13. Simulation analysis*

A Monte Carlo simulation study was carried out to evaluate the performance of the MLE of the parameter $\lambda$ in the NPEx distribution. Random samples were generated using the quantile-based algorithm described in Section 5.1.1. For each experiment, 1000 pseudo-random samples were generated for varying sample sizes and parameter values to assess both small-sample and asymptotic properties.

Sixteen parameter combinations were considered: $n = 50, 100, 500, 1000$ and $\lambda = 0.5, 1, 1.5, 2$. In each case, the MLE $\hat{\lambda}$ was obtained by maximizing the log-likelihood function in (41) using the `optim` routine in R with the BFGS method. Table 1 presents the average estimates (MLE), standard errors (SE), bias, and mean squared errors (MSE) over 1000 replications. The corresponding variation of bias and MSE across sample sizes is depicted in Figure 5.

Table 1 confirms the good performance of the MLE for the NPEx model. Both bias and MSE decrease with larger sample sizes, demonstrating estimator consistency and efficiency. The empirical SEs align with theoretical expectations, and coverage probabilities remain close to 95%, indicating reliable inference even for moderate samples.

**Table 1.** NPEx Simulation Results

| $\lambda$ | $n$ | MLE | SE | Bias | MSE | CP |
|---|---|---|---|---|---|---|
| 0.5 | 50 | 0.5082 | 0.0753 | 0.0082 | 0.00574 | 95.10 |
| | 100 | 0.5039 | 0.0551 | 0.0039 | 0.00305 | 94.50 |
| | 500 | 0.5007 | 0.0245 | 0.0007 | 0.00060 | 93.70 |
| | 1000 | 0.5010 | 0.0175 | 0.0010 | 0.00031 | 94.90 |
| 1.0 | 50 | 1.0181 | 0.1593 | 0.0181 | 0.02569 | 94.20 |
| | 100 | 1.0124 | 0.1075 | 0.0124 | 0.01170 | 95.70 |
| | 500 | 1.0035 | 0.0460 | 0.0035 | 0.00212 | 95.60 |
| | 1000 | 1.0003 | 0.0335 | 0.0003 | 0.00112 | 94.90 |
| 1.5 | 50 | 1.5275 | 0.2294 | 0.0275 | 0.05334 | 95.70 |
| | 100 | 1.5149 | 0.1597 | 0.0149 | 0.02571 | 95.00 |
| | 500 | 1.5078 | 0.0718 | 0.0078 | 0.00521 | 96.00 |
| | 1000 | 1.5014 | 0.0499 | 0.0014 | 0.00249 | 96.00 |
| 2.0 | 50 | 2.0524 | 0.3116 | 0.0524 | 0.09972 | 95.60 |
| | 100 | 2.0233 | 0.2135 | 0.0233 | 0.04609 | 95.20 |
| | 500 | 2.0028 | 0.0961 | 0.0028 | 0.00924 | 93.80 |
| | 1000 | 2.0015 | 0.0675 | 0.0015 | 0.00456 | 94.70 |

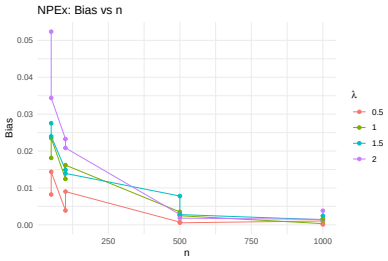


(a) Bias across sample sizes.

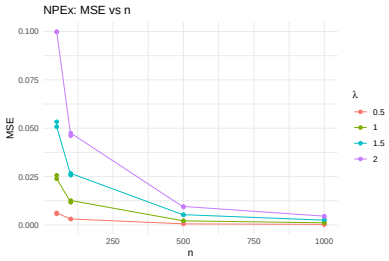


(b) MSE across sample sizes.

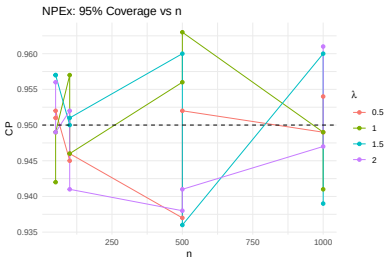


(c) Coverage probability (CP) across sample sizes.

**Figure 5.** Bias, mean squared error (MSE), and coverage probability (CP) plots of the NPEx model for different values of the rate parameter $\lambda$.

### *5.2. New Parsimonious Weibull (NPW) distribution*

The Weibull ($W$) distribution is widely used in reliability analysis and survival modeling due to its flexibility in representing different hazard shapes. Here, we adopt the baseline $W$ distribution with the *cdf*

$$F(y;\lambda,k) = 1 - e^{-(\lambda y)^k}, \qquad y > 0,\ \lambda > 0,\ k > 0.$$

Applying the proposed transformation, the *cdf*, *pdf*, and hazard rate function (hf) of the NPW model are obtained respectively as

$$G(y;\lambda,k) = \left[1 - e^{-(\lambda y)^k}\right] e^{\,e^{-(\lambda y)^k}}, \tag{44}$$

$$g(y;\lambda,k) = k\,\lambda^k y^{k-1} e^{-2(\lambda y)^k + e^{-(\lambda y)^k}}, \tag{45}$$

$$h(y;\lambda,k) = \frac{k\,\lambda^k y^{k-1} e^{-2(\lambda y)^k + e^{-(\lambda y)^k}}}{1 - \left[1 - e^{-(\lambda y)^k}\right] e^{\,e^{-(\lambda y)^k}}}. \tag{46}$$

Figures 6 and 7 show the density and hazard characteristics of the NPW model and its comparison with the Weibull baseline. The NPW distribution exhibits both unimodal and decreasing density shapes, while its hazard function displays flexible patterns such as increasing, decreasing, and bathtub forms. Compared with the Weibull model, NPW provides sharper *cdf* growth, heavier right skewness, and richer hazard dynamics—demonstrating its enhanced flexibility without added parameters.

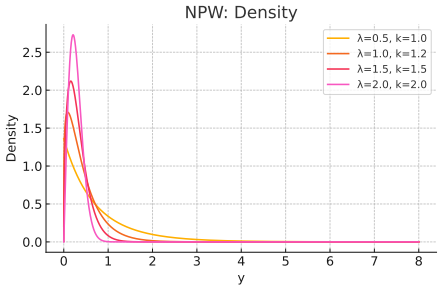


(a) NPW: Density.

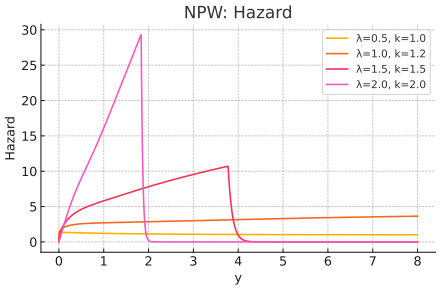


(b) NPW: Hazard.

**Figure 6.** NPW distribution: density and hazard functions for selected parameter combinations $(\lambda, k) \in \{(0.5, 0.7), (1.0, 1.0), (1.0, 1.5), (2.0, 2.0)\}$.

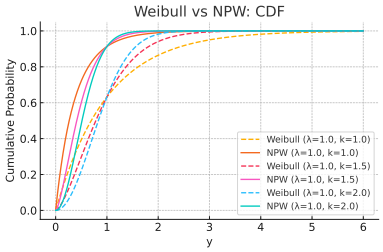


(a) Weibull vs NPW: CDF.

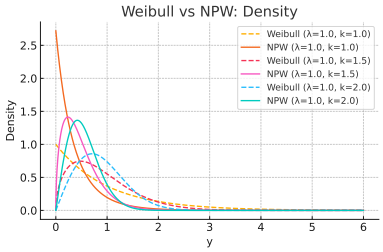


(b) Weibull vs NPW: Density.

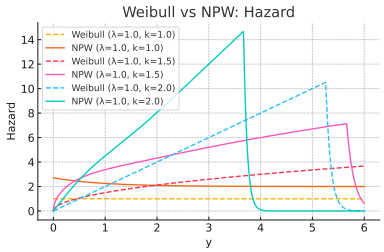


(c) Weibull vs NPW: Hazard.

**Figure 7.** Comparison between the Weibull and NPW distributions for selected parameter values $(\lambda, k) \in \{(1.0, 1.0), (1.0, 1.5), (1.0, 2.0)\}$. The plots illustrate cumulative distribution, density, and hazard rate differences.

### *5.2.1. Quantile function*

Let $u = F(y; \lambda, k)$ and $p = G(y; \lambda, k)$. From $p = u\, e^{\,1-u}$ we obtain

$$u = -\,W_0\!\left(-\frac{p}{e}\right),$$

where $W_0(\cdot)$ is the principal branch of the Lambert $W$ function. Solving $u = 1 - e^{-(\lambda y)^k}$ for $y$ yields the NPW quantile:

$$Q_G(p; \lambda, k) = \left\{ \frac{-\ln\!\big[1 + W_0(-p/e)\big]}{\lambda^{\,k}} \right\}^{1/k} = \frac{1}{\lambda}\left[-\ln\!\big\{1 + W_0(-p/e)\big\}\right]^{1/k}, \qquad 0 < p < 1. \tag{47}$$

*5.2.2. Random variate generation*

The inverse–transform sampler follows directly from (47):

(1) Generate $U \sim \text{Uniform}(0,1)$;
(2) Compute $u^* = -W_0(-U/e)$;
(3) Set $Y = \frac{1}{\lambda}\big[-\ln(1-u^*)\big]^{1/k}$.

Because $W_0$ is implemented in standard software, simulation is efficient and numerically stable. If $W_0$ is unavailable, one may instead solve $(1-e^{-(\lambda y)^k})e^{e^{-(\lambda y)^k}} - p = 0$ for $y$ using Newton–Raphson with the derivative

$$\frac{d}{dy}\Big\{(1-e^{-(\lambda y)^k})e^{e^{-(\lambda y)^k}}\Big\} = k\lambda^k y^{k-1}\, e^{-2(\lambda y)^k + e^{-(\lambda y)^k}}.$$

As $p \downarrow 0$, $W_0(-p/e) \to 0^-$ and $Q_G(p) \to 0$. As $p \uparrow 1$, $W_0(-p/e) \to -1^+$ and $Q_G(p) \to \infty$, so the support $(0,\infty)$ is preserved.

*5.2.3. Tail behavior and asymptotics*

Let $y \to \infty$ and define $s = (\lambda y)^k$ and $\varepsilon = e^{-s}$. Expanding $G(y) = F(y)e^{1-F(y)} = (1-\varepsilon)e^{\varepsilon}$ gives

$$G(y) = 1 - \tfrac{1}{2}\varepsilon^2 + O(\varepsilon^3) \quad \Rightarrow \quad \bar{G}(y) = 1 - G(y) = \tfrac{1}{2}e^{-2(\lambda y)^k}\,[1+o(1)].$$

Thus, the NPW survival tail decays faster than that of the Weibull distribution $\bar{F}(y) = e^{-(\lambda y)^k}$, implying a lighter right tail and reduced extreme-value sensitivity.

*5.2.4. Asymptotic hazard behavior*

Using $g(y) = f(y)e^{1-F(y)}[1-F(y)]$ and the expansion above, we have

$$g(y) \sim k\lambda^k y^{k-1} e^{-2(\lambda y)^k}, \qquad \bar{G}(y) \sim \tfrac{1}{2}e^{-2(\lambda y)^k}.$$

Hence, the hazard function satisfies

$$h_G(y) = \frac{g(y)}{\bar{G}(y)} \sim 2k\lambda^k y^{k-1} \quad (y \to \infty),$$

indicating that the NPW hazard approaches twice the Weibull hazard asymptotically.

*5.2.5. Stochastic ordering*

Since $W(u) = ue^{1-u}$ is increasing and concave on $(0,1)$, with $W(u) < u$, it follows that

$$G(y) = W(F(y)) < F(y) \quad \forall\, y > 0,$$

which implies the stochastic dominance relation

$$Y_{\text{NPW}} \leq_{\text{st}} Y_{\text{Weibull}}.$$

Furthermore, because $W'(u) = e^{1-u}(1-u)$ is decreasing, NPW also satisfies $Y_{\text{NPW}} \leq_{\text{hr}} Y_{\text{Weibull}}$ and $Y_{\text{NPW}} \leq_{\text{lr}} Y_{\text{Weibull}}$, showing it is smaller in hazard and likelihood ratio orderings.

Finally, NPW preserves scale closure: for $c > 0$, if $Y \sim \text{NPW}(\lambda, k)$ then $cY \sim \text{NPW}(\lambda/c,\, k)$.

### *5.2.6. Estimation (NPW)*

Let $y_1, \ldots, y_n$ be i.i.d. from the NPW density $g(y; \lambda, k) = k\,\lambda^k y^{k-1} \exp\{-2(\lambda y)^k + e^{-(\lambda y)^k}\}$, $y > 0$, $\lambda > 0$, $k > 0$. Write $s_i = (\lambda y_i)^k = \lambda^k y_i^k$. The log–likelihood is

$$\ell(\lambda, k) = n \log k + nk \log \lambda + (k-1) \sum_{i=1}^{n} \log y_i - 2 \sum_{i=1}^{n} s_i + \sum_{i=1}^{n} e^{-s_i}.$$

The score components are

$$\frac{\partial \ell}{\partial \lambda} = \frac{k}{\lambda}\left[n - 2\sum_{i=1}^{n} s_i - \sum_{i=1}^{n} s_i e^{-s_i}\right], \qquad \frac{\partial \ell}{\partial k} = \frac{n}{k} + n \log \lambda + \sum_{i=1}^{n} \log y_i - \sum_{i=1}^{n} s_i \log(\lambda y_i)\big[2 + e^{-s_i}\big].$$

Closed-form solutions are unavailable; $(\hat{\lambda}, \hat{k})$ are obtained numerically by solving the score equations or maximizing $\ell(\lambda, k)$. For numerical stability and constraints, we recommend the reparameterization

$$\eta = \log \lambda, \qquad \xi = \log k,$$

and unconstrained optimization (e.g., BFGS/Newton) on $(\eta, \xi)$ with back-transforms $\lambda = e^{\eta}$, $k = e^{\xi}$. Standard errors follow from the inverse observed Fisher information, computed either analytically via the Hessian or numerically:

$$\text{SE}(\hat{\lambda}) = \sqrt{\big[\mathcal{I}^{-1}(\hat{\lambda}, \hat{k})\big]_{11}}, \qquad \text{SE}(\hat{k}) = \sqrt{\big[\mathcal{I}^{-1}(\hat{\lambda}, \hat{k})\big]_{22}}.$$

Wald confidence intervals use the usual normal approximation.

Good starting values can be obtained from the baseline Weibull MLEs fitted to the data (ignoring the transformation): $(\lambda^{(0)}, k^{(0)})$. Alternatively, set $k^{(0)}$ from the slope of the Weibull log–log plot and $\lambda^{(0)}$ from the median. We used `R optim` with $(\eta, \xi)$, tight convergence tolerances, and gradient supply for reliable performance.

### *5.2.7. Simulation Analysis*

To evaluate the performance of the MLEs for the parameters of the NPW distribution, a Monte Carlo simulation study was conducted. Samples of sizes $n = 50, 100$, and 500 were generated using the inverse transform sampling technique based on the NPW distribution, under various combinations of the shape parameter $k \in \{1.0, 1.5, 2.0\}$ and the rate parameter $\lambda \in \{0.5, 1.0\}$. For each parameter setting, 1000 replications were performed.

For every generated sample, the MLEs of $\lambda$ and $k$ were obtained numerically by maximizing the log-likelihood function using the BFGS optimization routine in `R`. The

empirical bias, MSE, and coverage probability (CP) of the 95% confidence intervals were computed as

$$\text{Bias}(\hat{\theta}) = \frac{1}{N}\sum_{i=1}^{N}(\hat{\theta}_i - \theta), \tag{48}$$

$$\text{MSE}(\hat{\theta}) = \frac{1}{N}\sum_{i=1}^{N}(\hat{\theta}_i - \theta)^2, \tag{49}$$

$$\text{CP}(\hat{\theta}) = \frac{1}{N}\sum_{i=1}^{N} I\big(\theta \in [\hat{\theta}_i - 1.96 \times \text{SE}(\hat{\theta}_i), \hat{\theta}_i + 1.96 \times \text{SE}(\hat{\theta}_i)]\big), \tag{50}$$

where $\text{SE}(\hat{\theta}_i)$ is the estimated standard error of the $i^{th}$ replication and $I(\cdot)$ denotes the indicator function.

The numerical results, summarized in Tables 2–3, show that the MLEs for both parameters are consistent and asymptotically unbiased. The bias and MSE decline rapidly with increasing $n$ ($n = 50, 100, 500$), and the empirical CPs remain close to the nominal 95% level, confirming the reliability of the estimated standard errors.

Figures 8 and 9 further illustrate the convergence trends of bias, MSE, and CP with increasing $n$. The MSE curves decay approximately at the rate of $1/n$, while the bias approaches zero, demonstrating the efficiency and stability of the MLEs. Notably, the MSE of $\hat{k}$ remains nearly invariant across different values of $\lambda$, indicating a weak dependence between the scale and shape parameters and confirming the separability of parameter effects in the NPW model.

**Table 2.** NPW distribution: Simulation results for the rate parameter ($\lambda$) showing MLE, standard error (SE), bias, MSE, and CP.

| $\lambda$ | $k$ | $n$ | MLE | SE | Bias | MSE | CP (%) |
|---|---|---|---|---|---|---|---|
| 0.5 | 1.0 | 50 | 0.5141 | 0.0812 | 0.0141 | 0.00678 | 95.90 |
| | | 100 | 0.5081 | 0.0608 | 0.0081 | 0.00376 | 94.50 |
| | | 500 | 0.5010 | 0.0261 | 0.0010 | 0.00068 | 94.60 |
| | 1.5 | 50 | 0.5124 | 0.0569 | 0.0124 | 0.00339 | 94.10 |
| | | 100 | 0.5061 | 0.0395 | 0.0061 | 0.00160 | 94.40 |
| | | 500 | 0.5008 | 0.0174 | 0.0008 | 0.00030 | 95.50 |
| | 2.0 | 50 | 0.5078 | 0.0425 | 0.0078 | 0.00186 | 92.80 |
| | | 100 | 0.5044 | 0.0290 | 0.0044 | 0.00086 | 94.70 |
| | | 500 | 0.5012 | 0.0127 | 0.0012 | 0.00026 | 95.20 |

The simulation results in Tables 2–3 confirm the efficiency and consistency of the MLEs for the NPW distribution. Both parameters exhibit decreasing bias and MSE as the sample size increases, with empirical and model-based SEs closely aligned. CPs for the nominal 95% confidence intervals remain close to the expected level, indicating accurate standard error estimation. The estimator performance improves rapidly for $n \geq 100$, suggesting stable inference even for moderate sample sizes.

**Table 3.** NPW distribution: Simulation results for the shape parameter ($k$) showing MLE, standard error (SE), bias, mean squared error (MSE), and coverage probability (CP).

| $\lambda$ | $k$ | $n$ | MLE | SE | Bias | MSE | CP (%) |
|---|---|---|---|---|---|---|---|
| 0.5 | 1.0 | 50 | 1.0225 | 0.1115 | 0.0225 | 0.01293 | 96.40 |
| | | 100 | 1.0153 | 0.0815 | 0.0153 | 0.00686 | 94.80 |
| | | 500 | 1.0012 | 0.0357 | 0.0012 | 0.00128 | 94.00 |
| | 1.5 | 50 | 1.5398 | 0.1835 | 0.0398 | 0.03521 | 93.50 |
| | | 100 | 1.5255 | 0.1204 | 0.0255 | 0.01513 | 94.70 |
| | | 500 | 1.5033 | 0.0525 | 0.0033 | 0.00276 | 93.90 |
| | 2.0 | 50 | 2.0676 | 0.2402 | 0.0676 | 0.06219 | 93.70 |
| | | 100 | 2.0362 | 0.1645 | 0.0362 | 0.02835 | 93.70 |
| | | 500 | 2.0026 | 0.0717 | 0.0026 | 0.00514 | 94.00 |

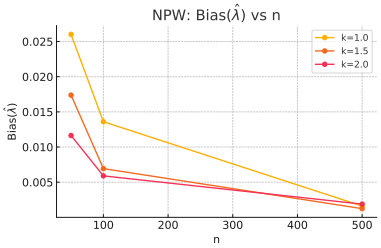


(a) Bias across $n$ (grouped by $k$).

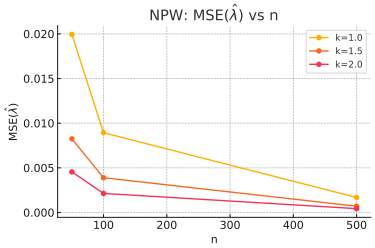


(b) MSE across $n$ (grouped by $k$).

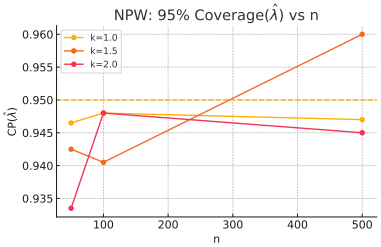


(c) 95% coverage across $n$ (grouped by $k$).

**Figure 8.** NPW simulation diagnostics for the rate parameter $\lambda$: bias, MSE, and 95% coverage as functions of sample size.

## 6. Real Data Analysis

This section evaluates the practical performance of the proposed parsimonious transformation using three distinct datasets that represent diverse hazard-rate topologies: monotonic increase (Dataset I), convex-to-concave transitions (Dataset II), and bathtub-shaped risk (Dataset III). Although these datasets are well-documented in the statistical literature, they are revisited here as benchmark stress-tests to assess whether the proposed parameter-free generator can flexibly capture complex hazard dynamics that typically require multi-parameter generalizations.

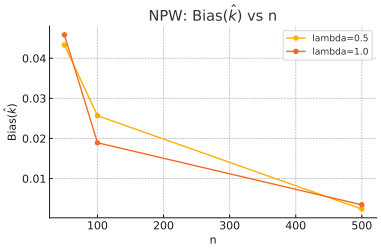


(a) Bias across $n$ (grouped by $\lambda$).

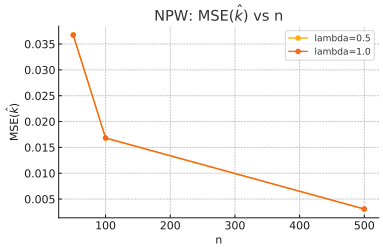


(b) MSE across $n$ (grouped by $\lambda$).

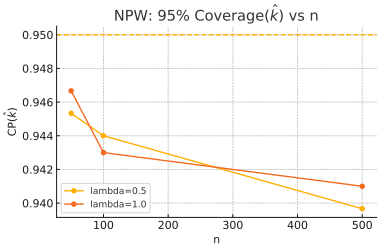


(c) 95% coverage across $n$ (grouped by $\lambda$).

**Figure 9.** NPW simulation diagnostics for the shape parameter $k$: bias, MSE, and 95% coverage as functions of sample size.

### *6.1. Data description and preliminary analysis*

**Dataset I:** The COVID-19 confirmed positive case data were collected from the state of Kerala, India, covering the period from March 9, 2020, to April 30, 2020. The data were published by the Government of Kerala through the official COVID-19 dashboard maintained by the Health and Family Welfare Department (`https://dashboard.kerala.gov.in/covid/daily.php`).

**Dataset II:** The Wheaton River flood peak exceedances data (in $m^3/s$) were originally reported by [7] and later analyzed in [6, 21]. It contains 72 observations from the Yukon Territory, Canada, recorded between 1958 and 1984.

**Dataset III:** The third dataset, recently examined in [17], includes the survival times (in weeks) of 33 patients diagnosed with acute myelogenous leukemia, providing insight into lifetime behavior in clinical survival studies.

To explore the underlying hazard characteristics, the Total Time on Test (TTT) plots shown in Figure 10 were constructed following the approach of [1]. Descriptive statistics, including measures of skewness and kurtosis, are reported in Table 4.

The TTT plot for Dataset I (COVID-19 data) displays a concave pattern, indicating an increasing failure rate (IFR). Consequently, the NPGu distribution was fitted, yielding a Kolmogorov–Smirnov (K–S) $p$-value of 0.7977, suggesting an excellent fit. The fitted density, empirical *cdf*, P–P plot, and survival function are shown in Figure 14.

The TTT plot for Dataset II exhibits a convex-to-concave transition, characteristic of a bathtub-shaped hazard function, motivating the use of the NPW distribution. Similarly, Dataset III (leukemia survival data) reveals a comparable hazard pattern and was modeled using the NPEx distribution. Figures 15 and 16 present the corresponding goodness-of-fit diagnostics.

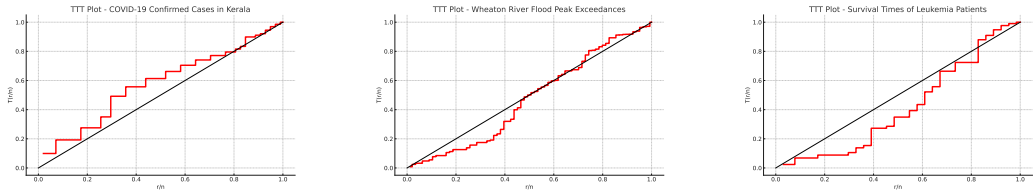


(a) Dataset I: COVID-19 confirmed cases (Kerala).

(b) Dataset II: Wheaton River flood peak exceedances.

(c) Dataset III: Leukemia patient survival times.

**Figure 10.** Total Time on Test (TTT) plots for the three datasets representing distinct hazard topologies: increasing (a), convex–concave (b), and bathtub-shaped (c) hazard rates.

**Table 4.** Descriptive Statistics.

| Dataset | I | II | III |
|---|---|---|---|
| Mean | 10.08 | 12.20 | 40.878 |
| Median | 8 | 9.50 | 22 |
| Mode | 2 | 1.70 | 4 |
| SD | 8.21 | 12.21 | 46.703 |
| Minimum | 1 | 0.10 | 155 |
| Maximum | 39 | 64 | 1 |
| Q1 | 4 | 2.13 | 4 |
| Q3 | 12 | 20.13 | 65 |
| IQR | 8 | 18 | 156 |
| Skewness | 1.52 | 1.47 | 1.165 |
| Kurtosis | 2.45 | 2.89 | 0.122 |

### *6.2. Exploratory Visualization*

To gain further insight into the structural patterns of the three datasets, graphical analyses were conducted through histograms, boxplots, kernel-density estimates, and empirical distributions, as shown in Figures 11–13. These exploratory plots provide a preliminary understanding of the data's distributional form, central tendency, and tail behavior, guiding the subsequent model-fitting process.

For Dataset I, the histogram and kernel-density plots exhibit strong right skewness with a heavy upper tail, while the boxplot confirms substantial variability and outliers. These features indicate a continuously increasing hazard pattern, consistent with the concave TTT curve, and justify the selection of the NPGu distribution to capture monotonic growth behavior.

For Dataset II, the data show a moderate right skew and extended tail. The density and time-series plots reveal intermittent peaks separated by quiet intervals, implying periods of low followed by high risk. This pattern supports the presence of a convex-to-concave, bathtub-shaped hazard function, motivating the NPW distribution as a suitable model.

For Dataset III, the distribution is right-skewed with relatively few long survivors, suggesting an early high risk that gradually declines before increasing again. This shape is characteristic of a decreasing-then-increasing hazard rate, making the NPEx distribution an appropriate candidate. The kernel-density and empirical *cdf* plots align

well with this interpretation.

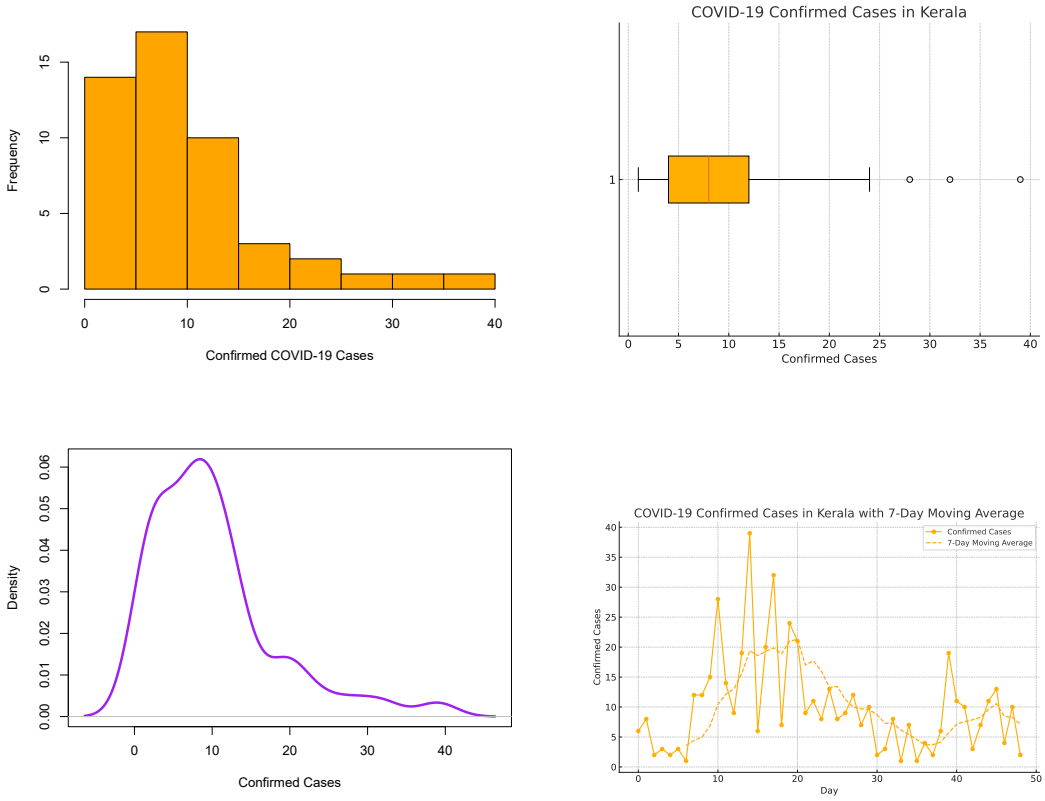


**Figure 11.** Dataset I: Histogram, boxplot, kernel density, and moving average plots for COVID-19 confirmed cases (Kerala).

### *6.3. Model Selection Criteria*

Before proceeding with the empirical fitting, we outline the statistical criteria employed to compare the performance of the proposed models with existing alternatives. The assessment relies on four well-established information-based measures and the Kolmogorov–Smirnov (K–S) goodness-of-fit test. These tools jointly evaluate both model adequacy and parsimony.

#### *6.3.1. Akaike Information Criterion (AIC)*

Introduced by [2], the AIC is defined as

$$AIC = 2k - 2\log(L(\boldsymbol{\zeta}; x)), \tag{51}$$

where $k$ denotes the number of estimated parameters and $L(\boldsymbol{\zeta}; x)$ is the maximized likelihood function. A smaller AIC indicates a model that achieves a better trade-off between goodness-of-fit and model complexity.

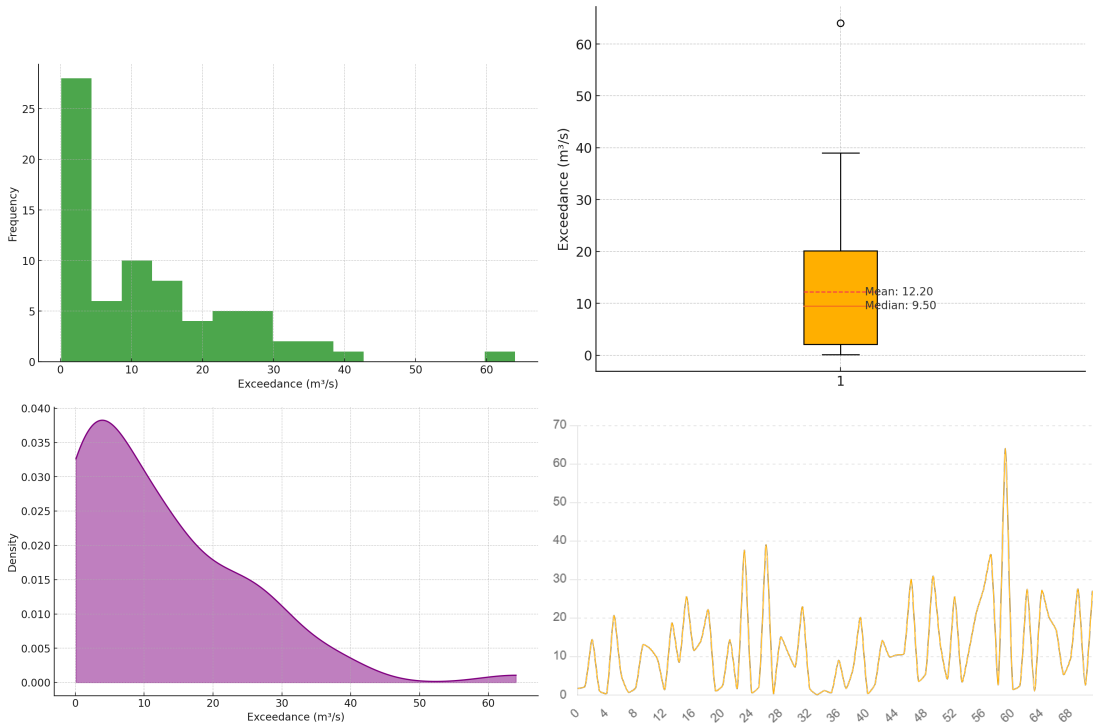


**Figure 12.** Dataset II: Histogram, boxplot, kernel density, and time-series plots for Wheaton River flood peak exceedances.

### *6.3.2. Bayesian Information Criterion (BIC)*

Proposed by [24], the BIC penalizes model complexity more heavily than AIC:

$$BIC = k\log(n) - 2\log(L(\boldsymbol{\zeta}; x)), \tag{52}$$

where $n$ is the sample size. The model with the lowest BIC is considered the most plausible under Bayesian asymptotic reasoning.

### *6.3.3. Consistent Akaike Information Criterion (CAIC)*

The CAIC, introduced to address potential overfitting in small samples, modifies the AIC penalty term as

$$CAIC = AIC + \frac{2k(k+1)}{n-k-1}. \tag{53}$$

This adjustment increases the penalty for complex models, improving selection consistency as $n$ grows.

### *6.3.4. Hannan–Quinn Information Criterion (HQIC)*

Proposed by [12], HQIC applies a milder penalty than BIC:

$$HQIC = 2k\log(\log(n)) - 2\log(L(\boldsymbol{\zeta}; x)). \tag{54}$$

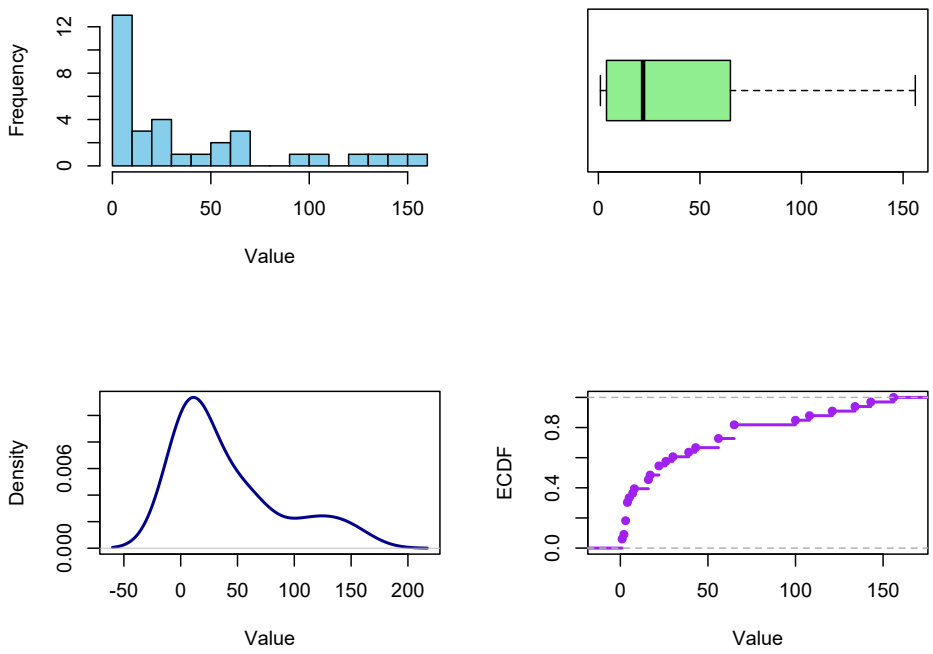


**Figure 13.** Dataset III: Histogram, boxplot, density plot, and empirical cumulative distribution (ECDF) for leukemia survival times.

This measure provides a compromise between the AIC's tendency toward overfitting and BIC's stronger penalty.

#### *6.3.5. Kolmogorov–Smirnov (K–S) test*

To further assess model adequacy, we apply the K–S statistic to measure the maximum absolute difference between empirical and fitted cumulative distribution functions:

$$D = \sup_x |F_n(x) - F(x; \hat{\boldsymbol{\zeta}})|. \tag{55}$$

A higher $p$-value indicates closer alignment between the empirical data and the fitted model.

In the subsequent subsection, these criteria are applied to compare the fitted NPGu, NPW, and NPEx models against several benchmark distributions. The combination of likelihood-based and distance-based measures ensures both goodness-of-fit and model efficiency are comprehensively evaluated.

### *6.4. Model Fitting and Comparison*

In this subsection, the proposed submodels-NPGu, NPW, and NPEx are fitted to the respective datasets using the MLE method. The goodness-of-fit is evaluated through a suite of information-based criteria, including the AIC, BIC, CAIC, and HQIC, alongside the K–S test statistic. Lower information-criterion values and higher $p$-values from

the K–S test indicate superior model adequacy.

### *6.4.1. Dataset I*

Table 5 and Figure 14 show the fitting results for the COVID-19 case data. Among all compared models, the NPGu distribution achieves the smallest AIC, BIC, HQIC, and CAIC values, together with the highest K–S $p$-value (0.7977), confirming its superior fit. The fitted density and survival plots closely match the empirical behavior, effectively capturing the monotonic increase in hazard rates during the observed period. Competing models, including the Normal, Logistic, and beta-Gumbel (betaGu) distributions [20], exhibit inferior fit quality, validating the structural efficiency of NPGu.

### *6.4.2. Dataset II*

For the flood peak exceedance data, Table 6 and Figure 15 summarize the model comparison results. The NPW model exhibits the lowest AIC (507.64) and smallest K–S statistic (0.1043), outperforming several multi-parameter competitors such as Kavya-Manoharan exponential (KME) [14], DUS exponential (DUSE) [15], SS-Exponential (SSE) [15], GDUS-Exponential (GDUSE) [18], Exponentiated Generalized Gumbel (EGGu) [9], and Kumaraswamy Pareto (KwPa) [6]. The fitted plots reveal that NPW successfully reproduces the convex–concave (bathtub-like) hazard pattern observed in the TTT plot. This result highlights the capacity of the NPW model to offer enhanced flexibility without parameter proliferation.

### *6.4.3. Dataset III*

The NPEx distribution is compared with Burr XII (BXII), Topp-Leone-BXII (TL-BXII), Marshall-Olkin-BXII (MOBXII), Zografos-Balakrishnan-BXII (ZBBXII), five-parameter beta-BXII (FBBXII), Beta-BXII (BBXII), Beta exponentiated-BXII (BE-BXII), five-parameter Kumaraswamy-BXII (FKwBXII), and the KwBXII distribution, which were recently studied and reported in [17] using the same dataset. The comparison results, given in Table 7 and Figure 16, indicate that the NPEx distribution provides the smallest information-criterion scores, despite being a two-parameter model. The fitted hazard curve exhibits the characteristic bathtub pattern, confirming that the NPEx distribution effectively captures non-monotonic hazard shapes with minimal model complexity.

**Table 5.** Dataset I: Model comparison using information criteria and K–S test.

| **Model** | **Parameters** | **-log$\ell$** | **AIC** | **BIC** | **HQIC** | **CAIC** | **K–S $p$-value** |
|---|---|---|---|---|---|---|---|
| **NPGu** | ($\hat{\mu} = 12.4078$, $\hat{\sigma} = 9.0727$) | **165.07** | **334.14** | **337.92** | **335.57** | **339.92** | **0.7977** |
| Normal | ($\hat{\mu} = 6.645$, $\hat{\sigma} = 5.468$) | 172.19 | 348.37 | 352.16 | 349.81 | 354.16 | 0.1375 |
| Logistic | ($\hat{\mu} = 7.187$, $\hat{\sigma} = 3.664$) | 170.36 | 342.73 | 346.51 | 344.17 | 348.51 | 0.3545 |
| betaGu | ($\hat{\mu} = 8.860$, $\hat{\sigma} = 7.067$, $\hat{a} = 0.935$, $\hat{b} = 1.337$) | 164.14 | 336.27 | 343.84 | 339.14 | 347.84 | 0.3328 |

Across the three empirical studies, the proposed parsimonious family demonstrated strong flexibility and competitiveness when compared with established multi-parameter models. The NPGu model provided an excellent fit to the COVID-19 dataset, capturing the increasing hazard pattern with the lowest AIC, BIC, and K–S statistics among the competitors. Similarly, the NPW model successfully modeled the

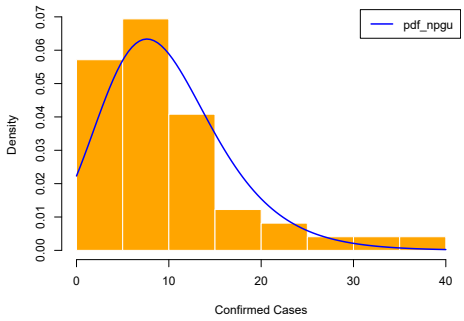


(a) Fitted histogram with NPGu overlay.

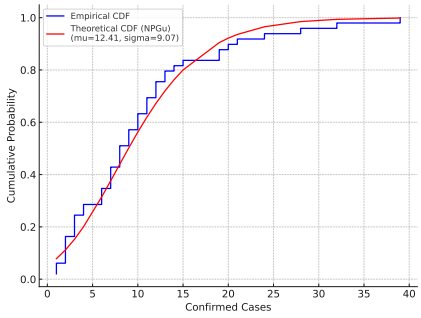


(b) Empirical and fitted CDFs.

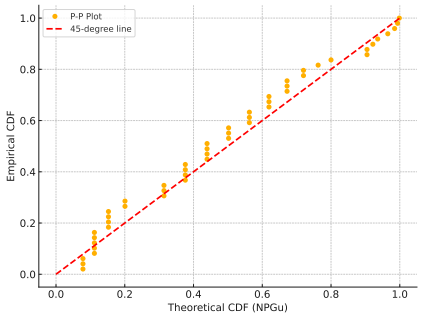


(c) P–P plot assessing distributional fit.

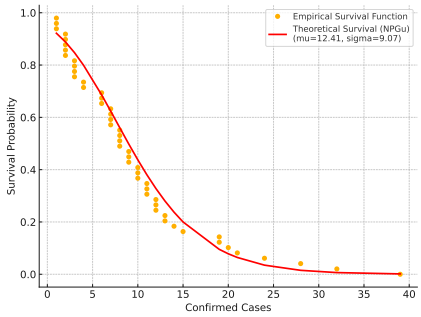


(d) Empirical survival and fitted NPGu curve.

**Figure 14.** Dataset I (COVID-19 cases, Kerala): Graphical assessment of fit under the NPGu model. The close alignment across all diagnostic plots supports the adequacy of the NPGu distribution.

**Table 6.** Dataset II: Model comparison for flood exceedance data.

| **Model** | **Parameters** | **log$\ell$** | **AIC** | **BIC** | **HQIC** | **K–S** |
|---|---|---|---|---|---|---|
| **NPW** | $(\hat{\lambda} = 0.0315,\ \hat{k} = 0.9333)$ | **-251.82** | **507.64** | **507.35** | **507.60** | **0.1043** |
| KME | $(\hat{\lambda} = 0.0632)$ | -252.01 | 506.03 | 508.30 | 507.18 | 0.110 |
| DUSE | $(\hat{\theta} = 0.0999)$ | -254.47 | 510.94 | 513.21 | 511.68 | 0.186 |
| SSE | $(\hat{\theta} = 0.0450)$ | -252.98 | 507.96 | 510.24 | 508.92 | 0.161 |
| GDUSE | $(\hat{\alpha} = 0.6803,\ \hat{\lambda} = 0.0812)$ | -251.62 | 507.25 | 511.80 | 508.92 | 0.113 |
| EGGu | $(\hat{\alpha} = 0.0988,\ \hat{\beta} = 0.4769,\ \hat{\mu} = 2.6317,\ \hat{\sigma} = 1.6639)$ | -256.89 | 521.80 | 530.88 | 525.72 | 0.108 |
| KwPa | $(\hat{a} = 2.855,\ \hat{b} = 85.847,\ \hat{k} = 0.0528,\ \hat{\beta} = 0.1)$ | -271.20 | 584.40 | 555.30 | 570.85 | 0.170 |

bathtub-shaped hazard observed in the Wheaton River flood data, outperforming all classical Weibull-based extensions despite its reduced parameterization. Finally, the NPEx model accurately characterized the leukemia survival dataset, yielding superior goodness-of-fit metrics relative to a wide class of Burr XII-type generalizations.

Overall, these results confirm that the new parsimonious generator can replicate complex empirical hazard behaviors—such as increasing, decreasing, and bathtub-shaped trends. This finding emphasizes the model's robustness, interpretability, and practical utility, thereby validating the theoretical developments introduced in earlier sections and motivating its further use in applied reliability and survival analysis

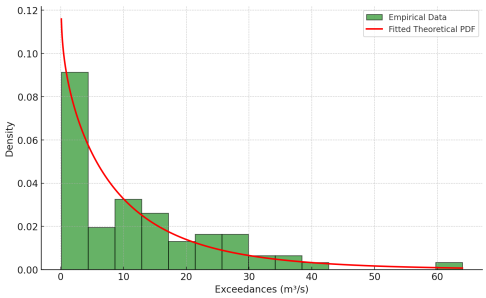


(a) Histogram with NPW overlay.

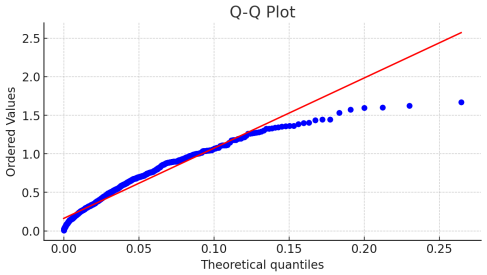


(b) Q–Q diagnostic plot.

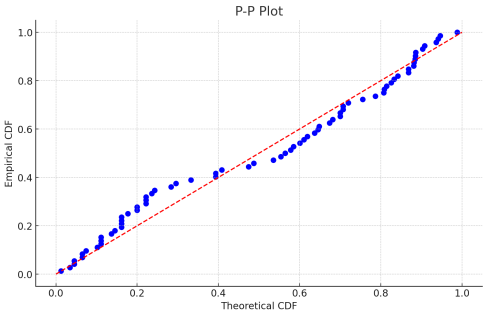


(c) P–P diagnostic plot.

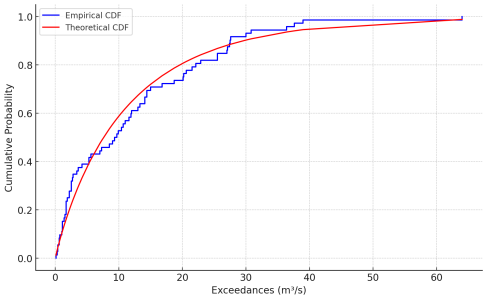


(d) Empirical and fitted CDFs.

**Figure 15.** Dataset II (Wheaton River flood exceedances): Diagnostic plots for NPW model fit, showing strong agreement between empirical and fitted distributions.

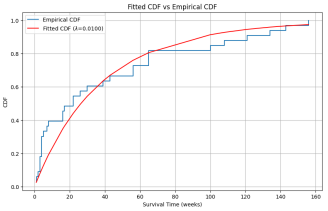


(a) Empirical and fitted CDFs.

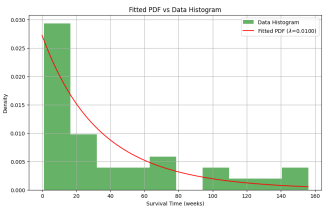


(b) Histogram with NPEx overlay.

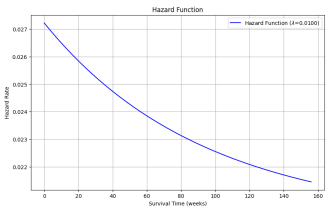


(c) Fitted hazard rate function.

**Figure 16.** Dataset III (Leukemia survival times): Fitted NPEx model showing excellent alignment with empirical data and clear bathtub-shaped hazard pattern.

**Table 7.** Dataset III: Comparison of NPEx with Burr-XII-type and related generalizations.

| Model | Parameters (MLE) | AIC | BIC | HQIC | CAIC |
|---|---|---|---|---|---|
| **NPEx** | ($\hat{\lambda} = 0.0100$) | **312.02** | **313.52** | **312.53** | **312.14** |
| Exponential | (0.0245) | 312.90 | 314.40 | 313.40 | 315.40 |
| Weibull | (0.776, 35.344) | 311.17 | 314.17 | 316.17 | 312.18 |
| BXII | (58.7, 0.006) | 328.21 | 331.19 | 328.61 | 329.20 |
| MOBXII | (11.838, 0.078, 12.25) | 315.54 | 320.01 | 316.38 | 317.04 |
| TLBXII | (0.281, 1.882, 50.215) | 316.30 | 320.73 | 317.09 | 317.76 |
| KwBXII | (9.201, 36.428, 0.242, 0.941) | 317.36 | 323.31 | 318.79 | 319.33 |
| BBXII | (96.10, 52.12, 0.10, 1.23) | 316.50 | 322.45 | 317.89 | 318.50 |
| BEBXII | (0.087, 5.007, 1.561, 31.270, 0.318) | 317.58 | 325.10 | 319.80 | 320.10 |
| FKwBXII | (14.7, 15.285, 0.29, 0.84, 0.03) | 317.76 | 325.20 | 319.98 | 320.27 |
| ZBBXII | (41.97, −0.16, 44.26) | 313.85 | 318.45 | 314.40 | 315.40 |

contexts.

## 7. Goodness of Fit Test

### *7.1. Nikulin–Rao–Robson (NRR) Statistic Test*

Goodness-of-fit testing verifies whether a theoretical model adequately represents observed data. Traditional tests such as Pearson's Chi-square may perform poorly when parameters are estimated from data or when samples are small or censored. The Nikulin–Rao–Robson (NRR) statistic [23] provides a modified Chi-square-type test that adjusts for parameter estimation and is particularly effective in reliability and survival contexts.

Let $H_0$ denote that a random sample $T_1, T_2, \ldots, T_n$ arises from $G(t;\boldsymbol{\zeta})$, where $\boldsymbol{\zeta}$ is a vector of unknown parameters. The sample space is divided into $r$ non-overlapping intervals with expected probabilities

$$p_j(\boldsymbol{\zeta}) = \int_{a_{j-1}}^{a_j} f(t;\boldsymbol{\zeta})\, dt, \quad j = 1, 2, \ldots, r, \tag{56}$$

and observed frequencies $\nu_j$. The NRR statistic is defined as

$$Y^2(\hat{\boldsymbol{\zeta}}) = X^2(\hat{\boldsymbol{\zeta}}) + \frac{1}{n}\boldsymbol{L}^T(\hat{\boldsymbol{\zeta}})\Big[\boldsymbol{I}(\hat{\boldsymbol{\zeta}}) - \boldsymbol{J}(\hat{\boldsymbol{\zeta}})\Big]^{-1}\boldsymbol{L}(\hat{\boldsymbol{\zeta}}), \tag{57}$$

where

$$X^2(\boldsymbol{\zeta}) = \sum_{j=1}^{r} \frac{(\nu_j - np_j(\boldsymbol{\zeta}))^2}{np_j(\boldsymbol{\zeta})}. \tag{58}$$

Here, $\boldsymbol{I}(\hat{\boldsymbol{\zeta}})$ is the Fisher information matrix, $\boldsymbol{J}(\hat{\boldsymbol{\zeta}})$ is the grouped-data information matrix, and $\boldsymbol{L}(\hat{\boldsymbol{\zeta}})$ accounts for the sensitivity of the grouped probabilities to parameter estimates. Under $H_0$, $Y^2(\hat{\boldsymbol{\zeta}})$ asymptotically follows a Chi-square distribution with $r-1$ degrees of freedom.

The NRR statistic shares conceptual similarities with classical tests such as the Kolmogorov–Smirnov (K–S) and Anderson–Darling (A–D) statistics, which also evaluate the discrepancy between theoretical and empirical distributions. However, unlike K–S and A–D tests, the NRR test explicitly incorporates the effect of parameter estimation through an information-based adjustment. This makes it particularly suitable for models with estimated parameters or grouped data, where standard tests may lose validity. Moreover, simulation studies confirm that the NRR statistic maintains stable Type I error rates and competitive power compared to K–S and A–D, while offering improved robustness for small or moderate sample sizes.

### *7.2. Simulation of the $\mathbf{Y^2}$ Statistic*

To validate the asymptotic behavior of the $Y^2$ statistic, Monte Carlo simulations were performed. For each configuration, 1000 random samples were generated from the NPGu distribution, with sample sizes $n = 50, 100, 200, 500$, and 800. The proportion of non-rejections of $H_0$ was evaluated at significance levels $\epsilon = 0.02, 0.05, 0.01$, and

0.1. The empirical and theoretical levels, shown in Table 8, exhibit close agreement, confirming the stability of the test under finite samples.

**Table 8.** Empirical and theoretical significance levels for the NRR test ($N = 1000$).

| $n$ | $\epsilon = 0.02$ | $\epsilon = 0.05$ | $\epsilon = 0.01$ | $\epsilon = 0.10$ |
|---|---|---|---|---|
| 50 | 0.982 | 0.945 | 0.990 | 0.920 |
| 100 | 0.984 | 0.947 | 0.993 | 0.914 |
| 200 | 0.983 | 0.946 | 0.986 | 0.891 |
| 500 | 0.983 | 0.956 | 0.991 | 0.889 |
| 800 | 0.981 | 0.951 | 0.990 | 0.901 |

Additionally, Figure 17 displays the empirical distribution of $Y^2$ under multiple parameter configurations, compared with the theoretical Chi-square distribution with $m = r - 1$ degrees of freedom. The close alignment across parameter values confirms that $Y^2$ converges to a Chi-square law asymptotically, supporting its distribution-free property.

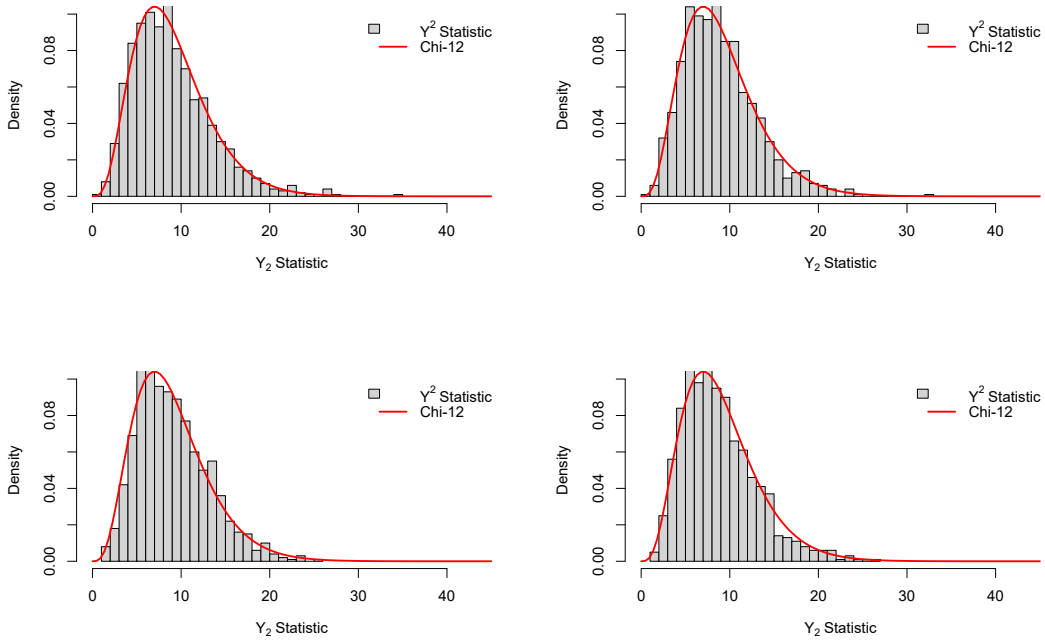


**Figure 17.** Simulated distributions of the $Y^2$ statistic under $H_0$ for different parameter values of the NPGu model, compared with the Chi-square(10) distribution ($n = 300$, $N = 1000$).

### *7.3. Application to the Kerala COVID-19 Data*

The NRR statistic was first applied to the COVID-19 dataset from Kerala, assuming the NPGu distribution under $H_0$. MLEs obtained via `optim` in R were $\hat{\mu} = 12.40783$

and $\hat{\sigma} = 9.07265$, yielding the estimated Fisher information matrix:

$$\mathbf{I}(\hat{\boldsymbol{\zeta}})^{-1} = \begin{bmatrix} 1.3363 & 0.7860 \\ 0.7860 & 1.1085 \end{bmatrix}.$$

The computed test statistic was $Y^2 = 7.0843$ with $r = 7$. At $\epsilon = 0.01$, the critical value $\chi^2_{0.01}(6) = 16.812$, and since $Y^2 < \chi^2_{0.01}(6)$, we fail to reject $H_0$. Thus, the NPGu model adequately fits the COVID-19 data.

### *7.4. Application to the Flood Data*

Applying the NRR test to the Wheaton River flood dataset under the NPW model produced MLEs $\hat{\lambda} = 0.03156$, $\hat{k} = 0.9333$, with Fisher information:

$$\mathbf{I}(\hat{\boldsymbol{\zeta}})^{-1} = \begin{bmatrix} 46540.794 & 6137.964 \\ 6137.964 & 128.3608 \end{bmatrix}.$$

Here, $Y^2 = 8.7889$ for $r = 9$. At significance level $\epsilon = 0.01$, $\chi^2_{0.01}(8) = 20.09$, confirming $Y^2 < \chi^2_{0.01}(8)$. Therefore, the NPW model is an appropriate fit for the flood exceedance data.

### *7.5. Application to the Survival Data*

Finally, the leukemia survival dataset was tested under the NPEx model, with MLE $\hat{\lambda} = 0.01005$ and $r = 11$. The resulting statistic $Y^2 = 13.7316$ was compared against $\chi^2_{0.01}(10) = 23.209$. Since $Y^2 < \chi^2_{0.01}(10)$, we fail to reject $H_0$, indicating that the NPEx distribution provides an adequate fit for the leukemia survival data.

## 8. Conclusion

This study introduced a parsimonious transformation within the T–X family, formulated through the generator $W(u) = ue^{1-u}$, providing a flexible yet parameter-preserving mechanism for extending baseline continuous distributions. Unlike conventional generalizations that increase flexibility by introducing additional shape parameters, the proposed transformation achieves comparable or superior adaptability by structurally modifying the weighting function of the cumulative distribution function. Comprehensive theoretical development established the core distributional, analytical, and reliability properties of the new family. Closed-form expressions were derived for key characteristics, including the probability density function, hazard rate, and moments. Structural analysis revealed that the transformation dynamically reallocates probability mass toward the lower tail, enabling the modeling of right-skewed and non-monotonic hazard behaviors without additional parameters. Monte Carlo simulations confirmed the statistical soundness of the maximum likelihood estimators and demonstrated consistent performance across different parameter settings and sample sizes. The simulation of the Nikulin–Rao–Robson ($Y^2$) statistic further validated its asymptotic Chi-square behavior, supporting its use as a robust goodness-of-fit measure for the proposed family. Empirical applications across three benchmark datasets—COVID-19 incidence data (NPGu), Wheaton River flood peak exceedances (NPW), and leukemia

survival times (NPEx)—illustrated the family's adaptability to a range of hazard rate structures, including monotonic, convex–concave, and bathtub-shaped forms. In each case, the new models achieved superior or competitive goodness-of-fit relative to several multi-parameter alternatives, while preserving interpretability and computational efficiency. In summary, the proposed transformation contributes a unifying, parsimonious framework for generating flexible lifetime and reliability models. Its demonstrated empirical strength and theoretical coherence position it as a promising alternative to conventional parameter-augmented generators. Future research could extend this approach to multivariate or truncated settings, develop Bayesian inferential procedures, and explore regression-type formulations for covariate-dependent hazard structures.

## Acknowledgement(s)

The authors express their sincere gratitude to the anonymous reviewers and the editorial board for their valuable comments and constructive suggestions, which have significantly improved the quality and clarity of this manuscript.

## References

[1] Aarset, M. V. (1987). How to identify a bathtub hazard rate. *IEEE transactions on reliability*, 36(1):106–108.

[2] Akaike, H. (1998). A bayesian analysis of the minimum aic procedure. In *Selected Papers of Hirotugu Akaike*, pages 275–280. Springer, Berlin, Heidelberg.

[3] Alzaatreh, A., Lee, C., and Famoye, F. (2013). A new method for generating families of continuous distributions. *Metron*, 71(1):63–79.

[4] Aryal, G. and Tsokos, C. P. (2009). Transmuted-g distributions: properties and applications. *Communications in Statistics – Theory and Methods*, 38(6):954–969.

[5] Baharith, L. A. and et al. (2018). New methods for generating families of distributions. *Mathematics*, 6(10):1–16.

[6] Bourguignon, M., Silva, R. B., Zea, L. M., and Cordeiro, G. M. (2013). The kumaraswamy pareto distribution. *Journal of Statistical Theory and Applications*, 12(2):129–144.

[7] Choulakian, V. and Stephens, M. A. (2001). Goodness-of-fit tests for the generalized pareto distribution. *Technometrics*, 43(4):478–484.

[8] Cordeiro, G. M. and de Castro, M. (2011). The kumaraswamy-g family of distributions: theory and applications. *Journal of Statistical Computation and Simulation*, 81(7):883–898.

[9] Cordeiro, G. M., Ortega, E. M., and da Cunha, D. C. (2013). The exponentiated generalized class of distributions. *Journal of data science*, 11(1):1–27.

[10] Elgarhy, M. et al. (2020). A parsimonious generator of continuous distributions. *Communications in Statistics – Simulation and Computation*. In press.

[11] Eugene, N., Lee, C., and Famoye, F. (2002). The exponentiated-g distribution family. *Communications in Statistics – Theory and Methods*, 31(4):497–512.

[12] Hannan, E. J. and Quinn, B. G. (1979). The determination of the order of an autoregression. *Journal of the Royal Statistical Society: Series B (Methodological)*, 41(2):190–195.

[13] Jones, M. C. (2004). The beta-g and related families of distributions. *Journal of Statistical Planning and Inference*, 126(1):25–54.

[14] Kavya, P. and Manoharan, M. (2021). Some parsimonious models for lifetimes and applications. *Journal of Statistical Computation and Simulation*, 91(18):3693–3708.

[15] Kumar, D., Singh, U., and Singh, S. K. (2015). A method of proposing new distribution and its application to bladder cancer patients data. *J. Stat. Appl. Pro. Lett*, 2(3):235–245.

[16] Manoharan, M. and Kavya, M. (2021). A new method for generating distributions: the

dus and kavya–manoharan models. *Journal of Statistical Distributions and Applications*, 8(1):1–18.
[17] Mansour, M. M., Ibrahim, M., Aidi, K., Shafique Butt, N., Ali, M. M., Yousof, H. M., and Hamed, M. S. (2020). A new log-logistic lifetime model with mathematical properties, copula, modified goodness-of-fit test for validation and real data modeling. *Mathematics*, 8(9):1508.
[18] Maurya, S., Kaushik, A., Singh, S., and Singh, U. (2017). A new class of distribution having decreasing, increasing, and bathtub-shaped failure rate. *Communications in Statistics-Theory and Methods*, 46(20):10359–10372.
[19] Merovci, F. (2013). Transmuted distributions and applications. *Communications in Statistics – Theory and Methods*, 42(9):1673–1691.
[20] Nadarajah, S. and Kotz, S. (2004). The beta gumbel distribution. *Mathematical Problems in engineering*, 2004(4):323–332.
[21] Nekoukhou, V. and Bidram, H. (2017). A new generalization of the weibull-geometric distribution with bathtub failure rate. *Communications in Statistics-Theory and Methods*, 46(9):4296–4310.
[22] R Core Team (2019). *R: A Language and Environment for Statistical Computing*. R Foundation for Statistical Computing, Vienna, Austria.
[23] Rao, K. C. and Robson, B. (1974). A chi-squabe statistic for goodies-of-fit tests within the exponential family. *Communications in Statistics-Theory and Methods*, 3(12):1139–1153.
[24] Schwarz, G. (1978). Estimating the dimension of a model. *The annals of statistics*, pages 461–464.
[25] Shaw, W. T. and Buckley, I. R. (2007). The transmuted distribution and related families. *Computational Statistics & Data Analysis*, 51(12):5997–6021.
[26] Zografos, K. and Balakrishnan, N. (2009). On generating continuous distributions via transformations. *Annals of the Institute of Statistical Mathematics*, 61(4):727–745.

## Appendices

## Appendix A.

**Table A1.** NPF Submodels with different supports.

| | **Distribution** | ***NPF*:Submodel** |
|---|---|---|
| Beta | $F(x;a,b) = I_x(a,b)$<br>$0 \le x \le 1$<br>$I_x(a,b)$ is the regularized incomplete beta function | G(x; a, b) $= I_x(a,b)e^{1-I_x(a,b)}$<br>$0 \le x \le 1$ |
| Br | $F(x;c,k) = 1-(1+x^c)^{-k}$<br>$c>0,\ k>0,\ x>0$ | $G(x;c,k) = \left[1-(1+x^c)^{-k}\right]e^{(1+x^c)^{-k}}$<br>$x>0$ |
| Gu | $F(x;\mu,\sigma) = e^{-e^{-\frac{(x-\mu)}{\sigma}}}$<br>$\mu>0, \sigma>0,\ x\in\mathbb{R}$ | $G(x;\mu,\sigma) = e^{-e^{-\frac{(x-\mu)}{\sigma}}}e^{1-e^{-e^{-\frac{(x-\mu)}{\sigma}}}}$<br>$x\in\mathbb{R}$ |
| Lo | $F(x;\mu,\sigma) = \frac{1}{1+e^{-\frac{(x-\mu)}{\sigma}}}$<br>$\mu$,$\sigma>0,\ x\in\mathbb{R}$ | $G(x;\mu,\sigma) = \frac{1}{1+e^{-\frac{(x-\mu)}{\sigma}}}e^{1-\frac{1}{1+e^{-\frac{(x-\mu)}{\sigma}}}}$<br>$x\in\mathbb{R}$ |
| PF | $F(x;\alpha,\beta) = \left(\frac{x}{\beta}\right)^{\alpha}$<br>$\alpha>0,\ \beta>0,\ 0\le x\le\beta$ | $G(x;\alpha,\beta) = \left(\frac{x}{\beta}\right)^{\alpha}e^{1-\left(\frac{x}{\beta}\right)^{\alpha}}$<br>$0\le x\le\beta$ |
| Pa | $F(x;\alpha,\beta) = 1-\left(\frac{\beta}{x}\right)^{\alpha}$<br>$\beta>0,\ \alpha>0,\ x\ge\beta$ | $G(x;\alpha,\beta) = \left[1-\left(\frac{\beta}{x}\right)^{\alpha}\right]e^{\left(\frac{\beta}{x}\right)^{\alpha}}$<br>$\beta>0,\ \alpha>0,\ x\ge\beta$ |